Volatility of Tornadogenesis: An Ensemble of Simulated Nontornadic and Tornadic Supercells in VORTEX2 Environments

BRICE E. COFFER AND MATTHEW D. PARKER

Department of Marine, Earth, and Atmospheric Sciences, North Carolina State University, Raleigh, North Carolina

JOHANNES M. L. DAHL

Atmospheric Science Group, Department of Geosciences, Texas Tech University, Lubbock, Texas

LOUIS J. WICKER AND ADAM J. CLARK

NOAA/OAR/National Severe Storms Laboratory, Norman, Oklahoma

(Manuscript received 30 May 2017, in final form 11 August 2017)

ABSTRACT

Despite an increased understanding of the environments that favor tornado formation, a high false-alarm rate for tornado warnings still exists, suggesting that tornado formation could be a volatile process that is largely internal to each storm. To assess this, an ensemble of 30 supercell simulations was constructed based on small variations to the nontornadic and tornadic environmental profiles composited from the second Verification of the Origins of Rotation in Tornadoes Experiment (VORTEX2). All simulations produce distinct supercells despite occurring in similar environments. Both the tornadic and nontornadic ensemble members possess ample subtornadic surface vertical vorticity; the determinative factor is whether this vorticity can be converged and stretched by the low-level updraft. Each of the 15 members in the tornadic VORTEX2 ensemble produces a long-track, intense tornado. Although there are notable differences in the precipitation and near-surface buoyancy fields, each storm features strong dynamic lifting of surface air with vertical vorticity. This lifting is due to a steady low-level mesocyclone, which is linked to the ingestion of predominately streamwise environmental vorticity. In contrast, each nontornadic VORTEX2 simulation features a supercell with a disorganized low-level mesocyclone, due to crosswise vorticity in the lowest few hundred meters in the nontornadic environment. This generally leads to insufficient dynamic lifting and stretching to accomplish tornadogenesis. Even so, 40% of the nontornadic VORTEX2 ensemble members become weakly tornadic. This implies that chaotic within-storm details can still play a role and, occasionally, lead to marginally tornadic vortices in suboptimal storms.

1. Introduction

Despite increased understanding of how environmental profiles of temperature, humidity, and winds affect the tornadic potential of convective storms, much is still unknown about what ultimately differentiates between seemingly similar nontornadic and tornadic supercells. Observations and simulations of nontornadic supercells show remarkable similarity to their tornadic counterparts, with operationally unobservable differences ultimately leading to tornadogenesis failure. While skill in tornado warnings has generally increased over time (Brooks 2004b), the false-alarm rate for tornadoes still hovers around 75% (Brotzge et al. 2011), despite warnings being correctly issued for environments known to be favorable for tornadoes based on the current state of the knowledge base (Anderson-Frey et al. 2016). As astutely pointed out by Anderson-Frey et al. (2016), the high false-alarm rate nationwide indicates that ''either our knowledge of the environmental controls on tornado formation is incomplete, or that there are factors beyond the environment that determine the differences between nontornadic and tornadic storms''.

To assess whether the failure point in nontornadic supercells could be specifically traced to some environmental trait that differs between the nontornadic and tornadic environments sampled during the second Verification of the Origins of Rotation in Tornadoes

Corresponding author: Brice Coffer, becoffer@ncsu.edu

DOI: 10.1175/MWR-D-17-0152.1

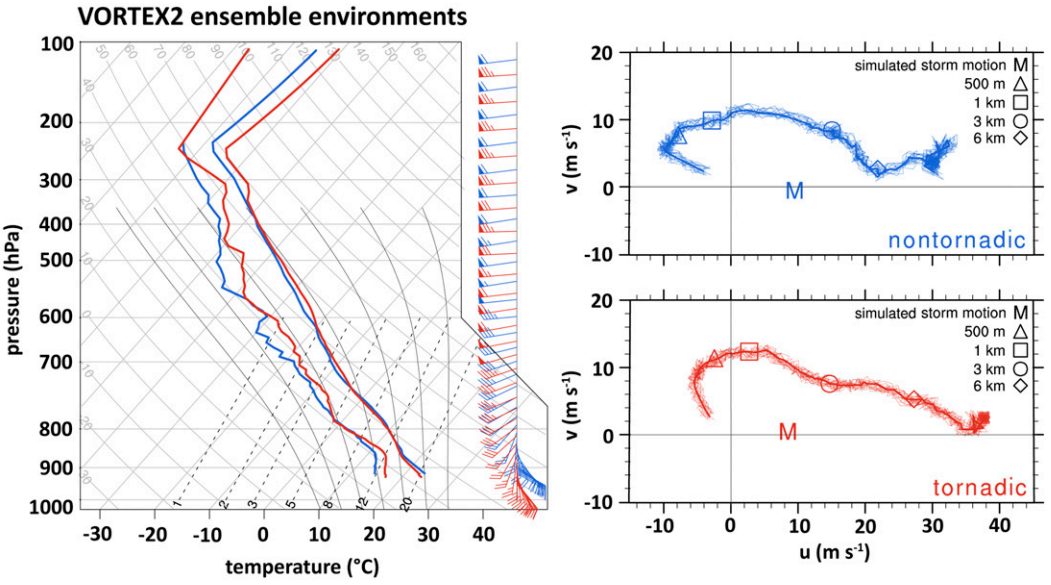

FIG. 1. (left) Skew T–log$p$ diagram and (right) hodographs showing the (top) nontornadic (blue) and (bottom) tornadic (red) VORTEX2 near-inflow composite soundings. The wind profiles for the 14 ensemble members are overlaid on the control wind profile (boldface) for both the nontornadic and tornadic hodographs. The simulated storm motion is indicated on the hodograph by the M. Markers on the hodograph represent 500 m (triangle), 1 km (square), 3 km (circle), and 6 km (diamond) AGL. The wind barbs on the skew T–log$p$ plot are displayed in kt (1 kt = 0.5144 m s^{-1}). See Parker (2014) for more discussion on the generation and interpretation of the VORTEX2 composite environments.

Experiment (VORTEX2; Wurman et al. 2012), Coffer and Parker (2017, hereinafter CP17) simulated supercells in the nontornadic and tornadic environments (Fig. 1) composited from soundings collected during VORTEX2 by Parker (2014). While the nontornadic and tornadic environments were both seemingly favorable for tornadoes by all conventional measures, there were key differences in the lower-tropospheric wind profile, specifically the orientation of the horizontal vorticity in the lowest few hundred meters above ground level (AGL). Increased streamwise horizontal vorticity and storm-relative helicity (SRH) in the lowest few hundred meters should promote a stronger low-level mesocyclone in a supercell and thereby stronger dynamic lifting. This lifting, in turn, may increase the likelihood of tornadogenesis (Markowski et al. 2012b; Markowski and Richardson 2014; Coffer and Parker 2015). Even though the nontornadic supercell in CP17 readily produced subtornadic[1] surface[2] vortices, these vortices failed to be stretched by the low-level updraft because of a disorganized low-level mesocyclone caused by the ingestion of predominately crosswise horizontal vorticity in the lowest few hundred meters AGL within the VORTEX2 nontornadic environment. In contrast, the tornadic supercell ingested predominately streamwise horizontal vorticity, which promoted a strong, steady low-level mesocyclone with enhanced dynamic lifting and stretching of surface vertical vorticity.

Further questions remain, however, including the complication that nontornadic and tornadic supercells can coexist side by side in nature (e.g., Klees et al. 2016). In other words, not all supercells in seemingly favorable environments are tornadic. This is an important operational forecasting issue that is not easily addressed with single sounding model studies. What is the range of outcomes in similar storms and environments? Is tornado formation strongly linked to the environment or primarily a volatile, stochastic process internal to each storm? Are the processes identified by CP17 common to a range of similar simulated storms (i.e., how robust were their findings)? The simulations of CP17 utilized the VORTEX2 composite environments directly from Parker (2014). It is certainly possible that those results were serendipitous (i.e., perhaps the VORTEX2 nontornadic environment produced a nontornadic supercell by chance). If tornadogenesis is stochastic, then our

[1] In this paper, "subtornadic vorticity" will refer to mesocyclonic scale vertical vorticity (≥0.01 s^{-1}) at the surface that is not (yet) associated with a tornado. Our definition of a tornadic vortex is discussed in section 2.

[2] In this paper, "surface," "near surface," or "near ground" will refer to ≤10 m AGL (the lowest model level grid point), while "low level" refers to ~1 km AGL, and "midlevel" refers to 3–7 km AGL.

TABLE 1. CM1 configuration.

Parameter	Description
Domain extent	200 km × 200 km × 18.16 km
Inner mesh	$\Delta x = \Delta y = 125$ m spanning 100 km × 100 km
Outer mesh	Stretching to $\Delta x = \Delta y = 4.875$ km (Wilhelmson and Chen 1982)
Vertical grid	115 levels starting at 10 m, $\Delta z = 20$ m below 300 m, stretching to $\Delta z = 280$ m at 12 km
Numerics	Third-order Runge–Kutta (RK3)/fifth-order weighted essentially nonoscillatory (WENO) advection of velocities and scalars (Wicker and Skamarock 2002)
Pressure solver	Klemp–Wilhelmson time splitting, vertically implicit (Klemp and Wilhelmson 1978)
Microphysics	NSSL two-moment (Ziegler 1985; Mansell 2010; Mansell et al. 2010)
Subgrid turbulence	TKE (Deardorff 1980) with separate horizontal and vertical coefficients
Bottom boundary condition	Semislip with $C_d = 0.0014$ (Coffer and Parker 2017)
3D initialization	Updraft nudging (Naylor and Gilmore 2012)

previous ''1 on 1'' comparison between the nontornadic and tornadic supercells may overstate the role of the ambient environment. We therefore wish to quantify where those particular simulations fall within a distribution of similar simulations.

Most model studies of tornadogenesis in supercells have only simulated a singular supercell. Very few studies have looked at a range of simulated storms in similar environments. Adlerman and Droegemeier (2005) briefly commented that small differences in the environmental wind profile led to distinct supercellular evolutions, specifically the rate of cyclic mesocyclogenesis. Naylor and Gilmore (2014) investigated storm-scale differences between supercells that produced tornadoes and those that did not using high-resolution simulations initialized with the Storm Prediction Center's (SPC) Rapid Update Cycle (RUC) database. They found that 37% of the ''tornadic'' soundings produced long-lived supercells that failed to generate a tornado, while 42% of their ''nontornadic'' soundings produced a tornadic strength vortex underneath the low-level mesocyclone. This suggests the possibility that a great deal of overlap exists between the range of outcomes for supercells, even in environments known to be favorable (or unfavorable) for tornadoes.

Markowski and Richardson (2017) explored the sensitivity of tornadogenesis to the location of a heat sink in ''toy model'' simulations. In an actual supercell, the heat sink represents the downdraft and the production of negatively buoyant air, which in turn may be affected by the deep-layer wind shear, storm-relative flow, hydrometer fall speeds, and hydrometeor species. Shifting the heat sink by only a few kilometers in any direction resulted in significant differences to the baroclinic generation of horizontal vorticity and subsequent surface vertical vorticity maxima. Thus, they concluded that even outflow with relatively small negative buoyancy combined with strong low-level dynamic upward forcing is insufficient (but necessary) for tornadogenesis. This volatility associated with downdraft position and strength may explain the failure of many actual supercells to produce tornadoes in seemingly favorable environments.

The main goals of this paper are to address the extent to which tornadogenesis is stochastic and to understand the range of possible outcomes in similar environments. To this end, we have completed an ensemble of 30 supercell simulations based on small variations from the VORTEX2 nontornadic and tornadic composite environmental profiles from Parker (2014) and CP17. If tornadogenesis is primarily linked to the environment, we would expect that the probability of tornadogenesis would vary distinctly between the VORTEX2 nontornadic and tornadic environments. This would mean that there are fundamental aspects of the respective environments (e.g., lower-tropospheric horizontal vorticity orientation) that are heavily determinative of tornadogenesis, notwithstanding the varying convective structures that arise as a result of the spread of the wind profiles within the ensemble. On the other hand, if instead tornadogenesis is primarily a stochastic process (i.e., highly dependent on random, unpredictable details within each storm), then we would expect that small perturbations to the respective nontornadic and tornadic wind profiles would lead to a wide range of outcomes in terms of tornado production. Such volatility would presumably be linked to differences in the evolution of convection in the simulated storms, including the presence–absence and timing of downdrafts, pockets of subtornadic surface vertical vorticity, or zones of strong dynamic lifting that provide the stretching needed for tornadogenesis. Probably, in reality, the environment exerts a substantial influence over the internal storm dynamics leading to tornadogenesis, even as chaotic within-storm details still permit a range of possible outcomes. However, to date there have been few attempts to constrain these two pieces of the

TABLE 2. Range of SRH ($m^2 s^{-2}$) values over various depths for the VORTEX2 ensemble profiles. SRH was calculated using the Bunkers storm motion (Bunkers et al. 2000), which was similar to the simulated storm motions. The effective inflow layer is described by Thompson et al. (2007).

	0–500-m SRH	0–1-km SRH	Effective SRH
Nontornadic	60–96	139–164	299–330
Tornadic	138–174	208–237	284–312

tornadogenesis puzzle. Here, we describe a sensitivity test aimed at understanding the robustness of our previously simulated nontornadic and tornadic supercells.

Section 2 reviews the numerical setup of the ensemble simulations performed herein. Results of the simulations are presented in section 3, while a discussion of the implications and avenues for future work are offered in section 4.

2. Methods

An ensemble of 30 supercell simulations, 15 each for the VORTEX2 nontornadic and tornadic composite environments, was conducted using a similar model configuration to that in CP17 with the following minor differences. Simulations were conducted using the latest release (18) of Cloud Model version 1 [CM1; Bryan et al. 2003, also see the appendix of Bryan and Morrison (2012)]; however, the National Severe Storms Laboratory (NSSL) microphysics scheme used herein was the same version as in CM1 release 17. The only other model configuration difference was the use of an adaptive time-step technique. The reasoning for employing the adaptive time step was twofold: first, computational efficiency; second, the near impossibility of predicting the most unstable member of the ensemble a priori. The control member of each VORTEX2 ensemble produced similar supercellular structures and evolution to that of CP17. A summary

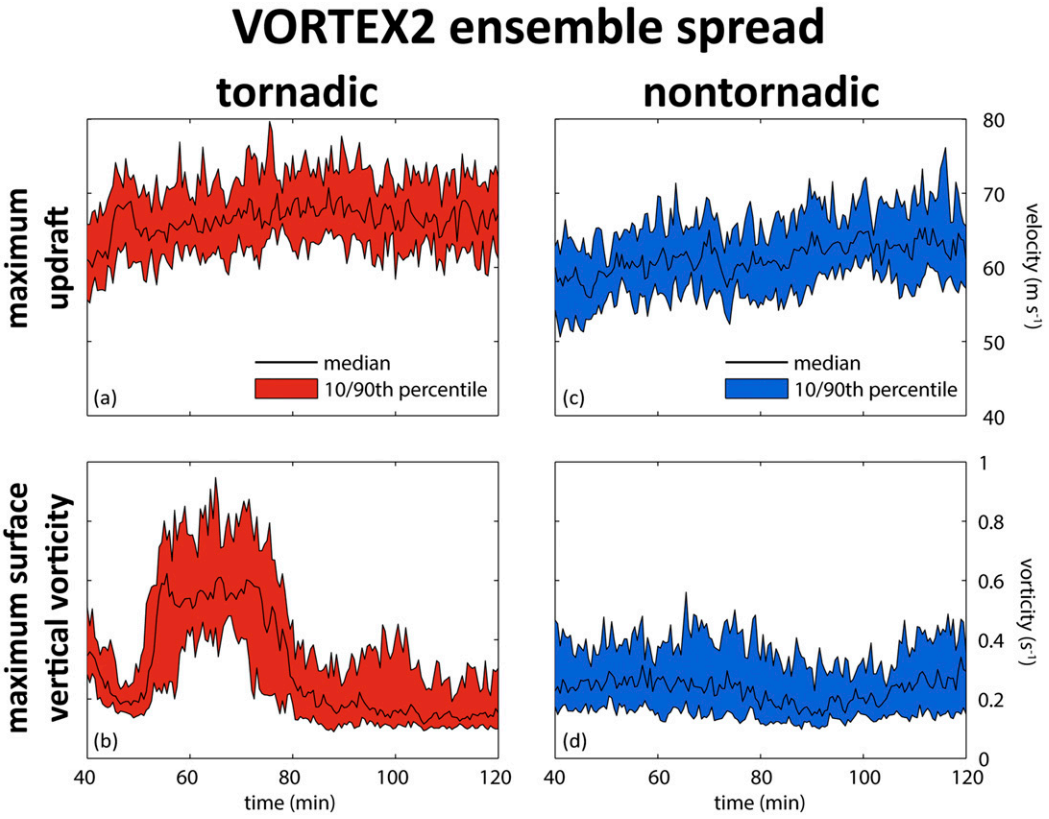

FIG. 2. Time series comparing the vertical velocity ($m s^{-1}$) and surface vertical vorticity (s^{-1}) for both the (a),(b) tornadic (red) and (c),(d) nontornadic (blue) VORTEX2 ensemble. (top) The median maximum vertical velocity value (black line) in both the (a) tornadic and (c) nontornadic VORTEX2 ensembles. (bottom) The median maximum surface vertical vorticity (black line) for the (b) tornadic and (d) nontornadic VORTEX2 ensembles. The shaded envelope covers the 10th and 90th percentiles for each ensemble. No smoothing or filtering was applied to the time series.

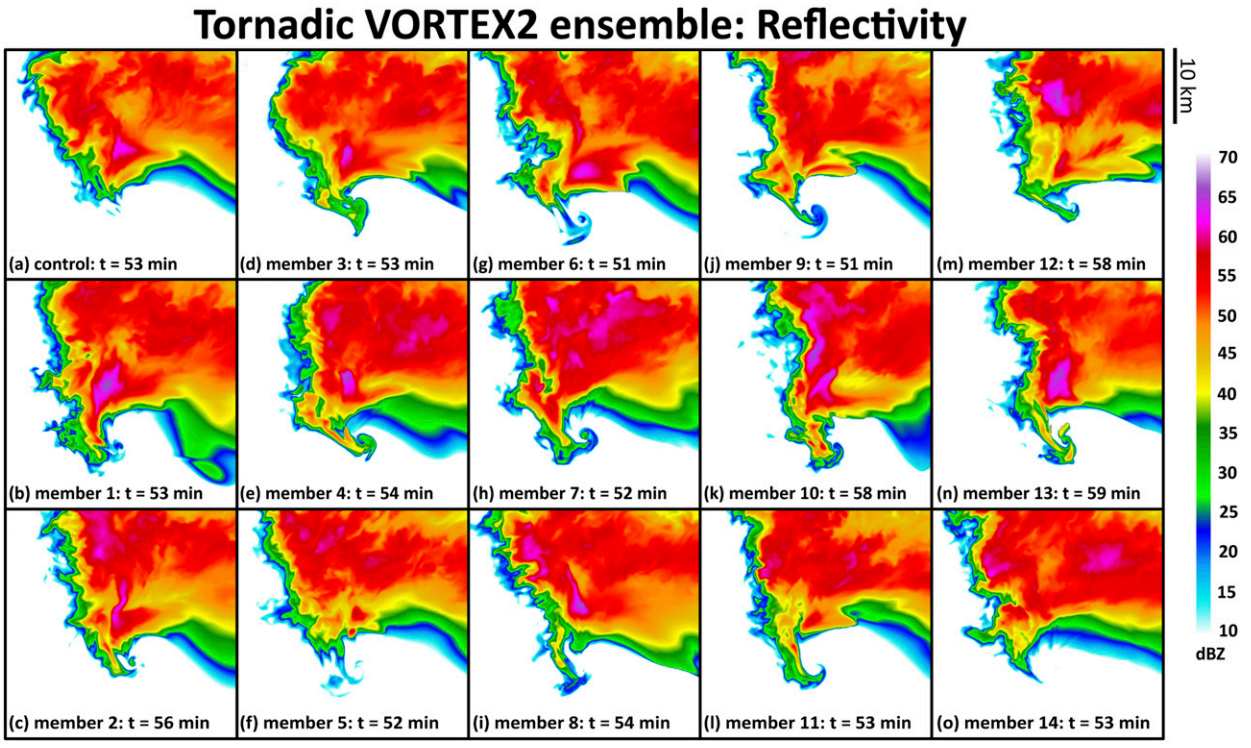

FIG. 3. Horizontal cross sections of 10 m AGL reflectivity (dBZ; shaded) at the key time period of tornadogenesis (indicated for each ensemble member in the corresponding panel) for the tornadic VORTEX2 ensemble.

of the CM1 configuration options can be found in Table 1. Of course, any of the subjective choices in the model configuration could affect the eventual volatility of tornadogenesis in the ensemble.

For each of the steady-state near-inflow VORTEX2 composite profiles from CP17, 14 ensemble members were initialized by applying horizontal wind perturbations generated from a uniform distribution with a maximum magnitude of 2 m s^{-1} to the wind profile, irrespective of height (Fig. 1). The horizontal wind perturbations were implemented using code from the National Severe Storms Laboratory Collaborative Model for Multiscale Atmospheric Simulation (NCOMMAS; Dowell and Wicker 2009; Dowell et al. 2011). The mean of the perturbations applied to each wind profile is practically zero, and the perturbations are identical between the corresponding members of the nontornadic and tornadic VORTEX2 ensembles. An additional control member for each VORTEX2 wind profile was simulated with no horizontal wind perturbations. No perturbations were added to the thermodynamic profile. The random wind perturbations are simply meant to represent random turbulence present in the atmosphere. The value of 2 m s^{-1} has been shown to be roughly the same order of magnitude as differences between wind profiles measured from nearby observational platforms (Dawson et al. 2012). The range of SRH values over various depths as a result of the wind perturbations is listed in Table 2, including 0–500-m SRH ranging from approximately 60 to 96 and 138 to 174 m^2 s^{-2} for the nontornadic and tornadic environments, respectively. The purpose of these small random perturbations was to produce a range of comparable, yet distinct storms in very similar environments. In this paper, the ensemble initialized with the nontornadic (tornadic) near-inflow VORTEX2 composite profile will be referred to as the nontornadic (tornadic) VORTEX2 ensemble. One of the goals of this paper is to determine if any of the "nontornadic" VORTEX2 ensemble members actually produce a tornado and whether any of the "tornadic" VORTEX2 ensemble members fail to.

For each ensemble member, a key time period of tornadogenesis or tornadogenesis failure was chosen based on several subjectively determined thresholds. Tornadogenesis was said to occur whenever all of the following criteria were met: 1) the surface vertical vorticity exceeds 0.3 s^{-1}, 2) the pressure deficit (relative to the base-state environmental sounding) within the vortex exceeds 10 hPa over a depth of at least 1 km, and 3) the instantaneous ground-relative wind speed exceeds 35 m s^{-1} (~78 mi h^{-1}, midrange EF0 wind speeds) at 10 m AGL. All of the criteria needed to be simultaneously present for

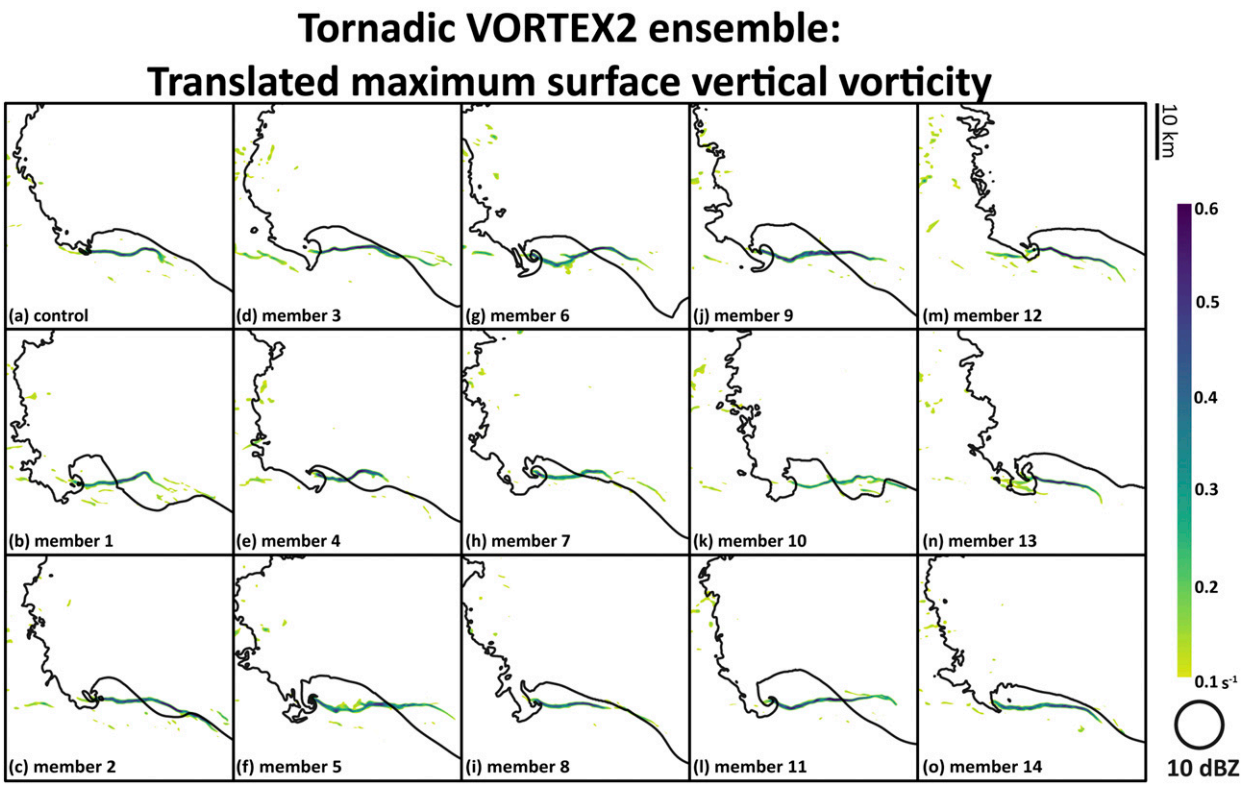

FIG. 4. Horizontal cross sections of 10 m AGL translated maximum vertical vorticity (s^{-1}; shaded) during the simulation. The 10-dBZ reflectivity contour (black) at 10 m AGL is shown for the respective ensemble members at the key time period of tornadogenesis for the tornadic VORTEX2 ensemble (refer to Fig. 3 for each ensemble member's key time index).

at least 2 min. If a supercell did not meet the tornadogenesis criteria at any point during the entire simulation, tornadogenesis failure was said to occur at the time of maximum surface vertical vorticity. The times of tornadogenesis or tornadogenesis failure were then used as benchmarks for comparisons among the 30 simulations. Most other analysis techniques are the same as those described by CP17. It should be noted that the grid spacing in these simulations is 125 m, and thus tornado-scale processes, which are often on the order of <100 m, could be underresolved. This has implications for the nontornadic VORTEX2 ensemble because weaker tornadoes tend to be associated with narrower path widths (Brooks 2004a). Despite not fully resolving tornadoes, this study presents a range of supercells with intense tornado-like vortices and is a positive step forward in not just focusing on one deterministic simulation, but rather the range of possibilities that are present within the same environment.

3. Results

For the first 20 min of each ensemble member, a large amount of precipitation forms in response to the updraft-nudging initialization technique, and relatively little spread develops while positive vertical velocities are enforced upon the model solutions. Afterward, in each ensemble member, a dominant, cyclonic, right-moving storm takes on supercellular reflectivity structures, and weaker disorganized convection moves north into the outer mesh. The ensemble members initialized with the tornadic VORTEX2 environment organize at low levels approximately 10 min sooner than the supercells in the nontornadic VORTEX2 ensemble. Each ensemble member contains storms with a strong midlevel updraft (Figs. 2a,c). During the final 80 min (t = 40–120 min) of the simulations, the tornadic VORTEX2 ensemble has a mean maximum updraft speed that is only 5 m s^{-1} larger than the nontornadic VORTEX2 ensemble (68 vs 63 m s^{-1}), consistent with the slight increase in convective available potential energy (CAPE; ~375 J kg^{-1}) in the tornadic VORTEX2 profile. However, the tornadic VORTEX2 ensemble has a mean maximum surface vertical vorticity that is nearly twice as high (0.91 vs 0.47 s^{-1}; Figs. 2b,d). While the bulk statistics for each ensemble indicate that the general trend is for the nontornadic environment to favor nontornadic supercells and the tornadic environment

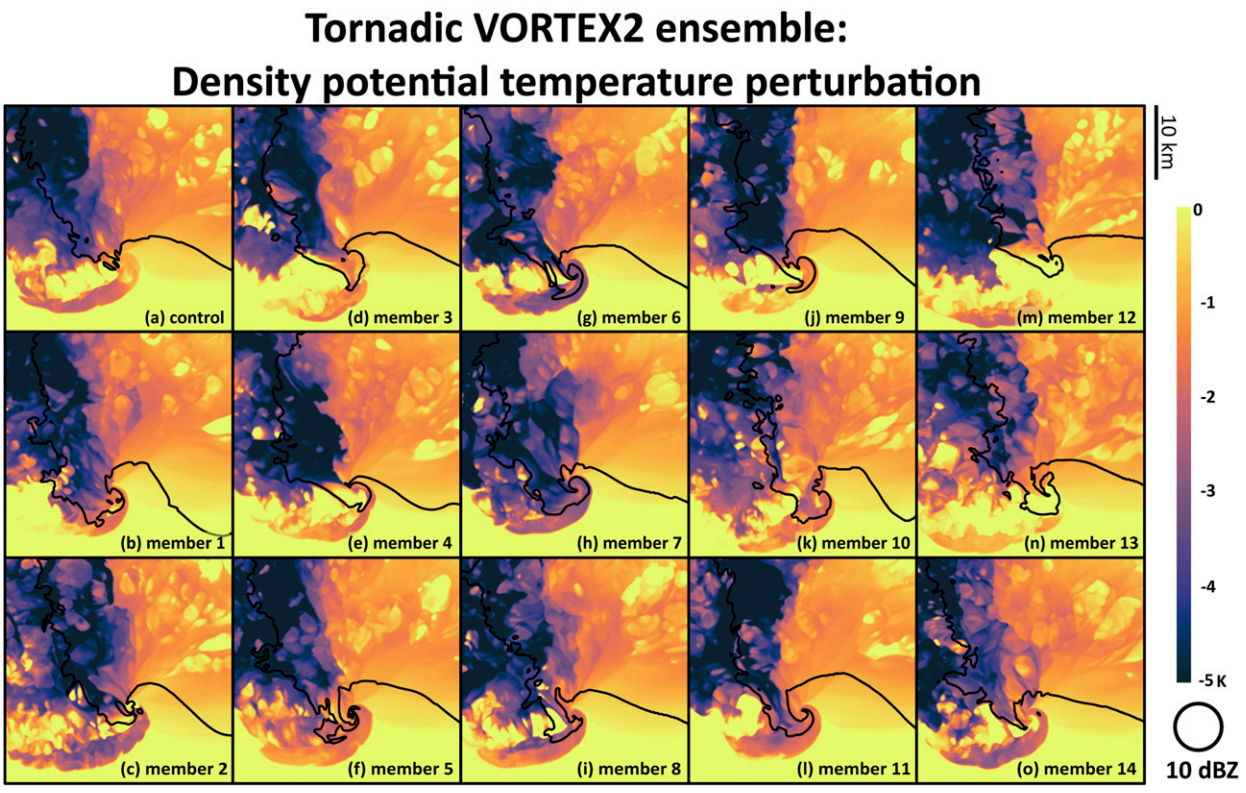

FIG. 5. Horizontal cross sections of 10 m AGL density potential temperature perturbation (K; shaded) at the key time period of tornadogenesis for the tornadic VORTEX2 ensemble. The 10-dBZ reflectivity contour (black) at 10 m AGL for the respective ensemble members is shown for reference (refer to Fig. 3 for each ensemble member's key time index). Density potential temperature perturbations are proportional to the buoyancy (Emanuel 1994).

to favor tornadic storms, there are unique features in each of the ensemble members. Some of the nontornadic VORTEX2 ensemble members are briefly tornadic, while in the tornadic VORTEX2 ensemble, individual members have varying surface buoyancy fields, yet still produce similarly intense tornadic vortices. We discuss these details in the following subsections, first for the tornadic VORTEX2 ensemble and then for the nontornadic VORTEX2 ensemble.

a. *Characteristics of the tornadic VORTEX2 ensemble*

All 15 members of the tornadic VORTEX2 ensemble produce surface vortices that clearly meet the criteria of tornadogenesis outlined in section 2. Genesis time ranges from $t = 51$ to 59 min (Fig. 3), with the maximum surface vertical vorticity for each member ranging from 0.65 to 1.12 s^{-1}. The tornadoes last for 17–32 min with pathlengths[3] approximately 15–30 km long (Fig. 4). Despite every member producing a tornado, each vortex has unique features, including various cycloidal paths and reaching peak intensity at different stages in their life cycles.

Even though the key time period of tornadogenesis is relatively tightly clustered around $t = 53$ min, each simulation produces a distinctly different supercell. The location and intensity of the main precipitation core differs between each ensemble member by the time of tornadogenesis, as well as the orientation and intensity of forward-flank precipitation (Fig. 3). Another notable difference between the supercells is the structure of the hook echo, specifically the intensity of precipitation in the vicinity of the developing low-level rotation (Fig. 3). For example, members 5 and 7 (Figs. 3f,h) undergo tornadogenesis at the same time in the simulation; however, member 5 has much less precipitation in the hook echo and has a gentler gradient of reflectivity across the forward flank.

The differences in precipitation lead to varying distributions of near-surface buoyancy (Fig. 5). A wide range of near-surface density potential temperatures is observed within a 2-km radius of each tornado, with

[3] Pathlength distances were calculated using the contour of time-integrated maximum vertical vorticity greater than 0.3 s^{-1}.

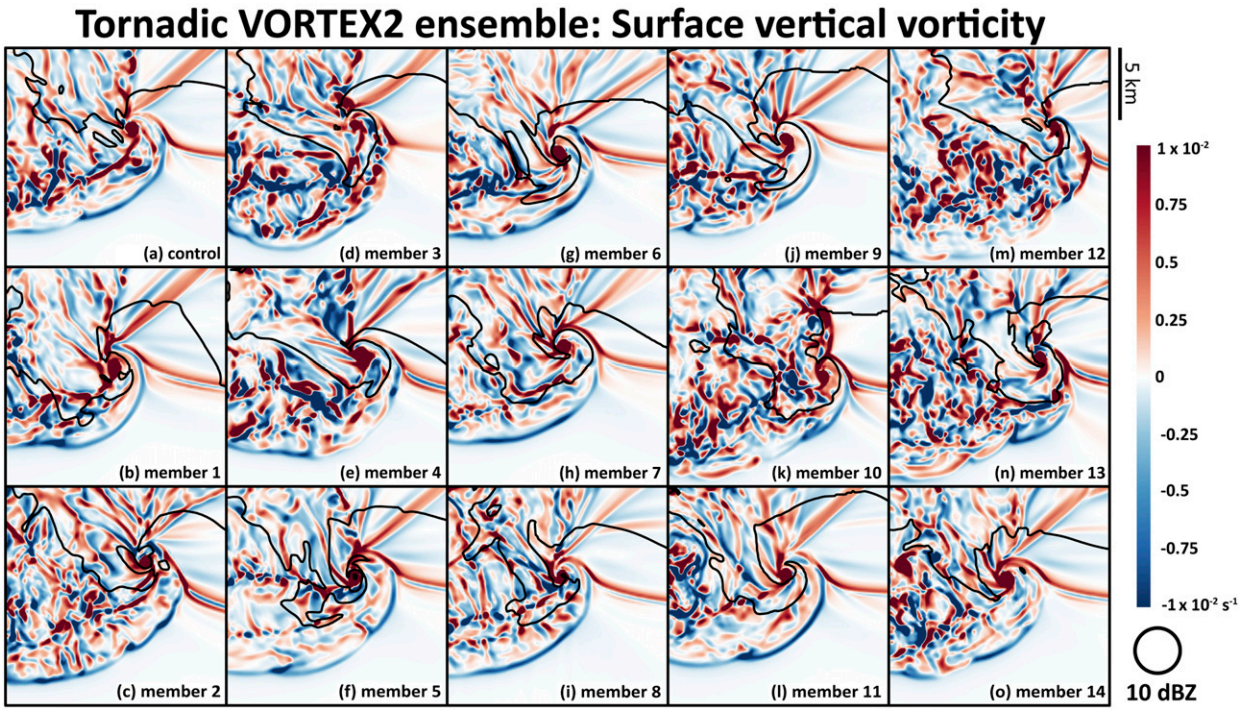

FIG. 6. Horizontal cross sections of 10 m AGL vertical vorticity (s^{-1}; shaded) at the key time period of tornadogenesis or tornadogenesis failure for the tornadic VORTEX2 ensemble. The 10-dBZ reflectivity contour (black) at 10 m AGL for the respective ensemble members is shown for reference (refer to Fig. 3 for each ensemble member's key time index).

maximum deficits ranging from approximately −1 to −6 K. For example, member 7 contains particularly cold air within the hook echo (Fig. 5h), while member 12 is quite warm (Fig. 5m). Internal surges in the rear-flank outflow (e.g., Marquis et al. 2008, 2012; Lee et al. 2012; Kosiba et al. 2013; Skinner et al. 2014; Schenkman et al. 2016; Orf et al. 2017) are present in every ensemble member throughout the lifetime of each tornado (not shown); however, in general, vortexgenesis in the tornadic VORTEX2 ensemble members occurs upon the initial development and arrival of the main cool outflow to a region of broad convergence underneath the intensifying low-level mesocyclone [similar to Markowski and Richardson (2014); also see the supplemental material of CP17 for animations of this process], even in members that have weak surface buoyancy near the hook echo at the key time period. Because of the differences in near-surface buoyancy, the subtornadic surface vertical vorticity field varies in each member (Fig. 6). At the time of tornadogenesis, there is a compact vortex near the hook echo in each supercell, yet the flow of air surrounding the vortex, including the presence of vorticity rivers (Dahl et al. 2014), varies from member to member.

Despite outflow temperature deficits that often exceeded what is typically found in significantly tornadic supercells (Markowski et al. 2003; Grzych et al. 2007), as mentioned earlier, each tornadic VORTEX2 ensemble member produces an intense tornadic vortex (Fig. 4). Both observations (e.g., Markowski 2002; Markowski et al. 2012a,b; Straka et al. 2007; Marquis et al. 2012) and simulations of tornadic supercells (e.g., Rotunno and Klemp 1985; Davies-Jones and Brooks 1993; Wicker and Wilhelmson 1995; Adlerman et al. 1999; Dahl et al. 2014; Markowski and Richardson 2014; Dahl 2015; Parker and Dahl 2015; Markowski 2016) have shown that baroclinicity is often a major contributor to the development of surface vertical vorticity. In the simulations analyzed by Markowski and Richardson (2017), small shifts in downdraft location greatly altered the development of near-surface cyclonic vorticity. Similar displacements in the low-level downdrafts are present within the tornadic VORTEX2 ensemble (Fig. 7). Consistent with the differences in precipitation structure, the location and intensity of downdrafts within each storm vary. There is no clear relationship between maximum surface vertical vorticity and maximum intensity of the downdraft nor the outflow temperature in the immediate vicinity of the hook echo (not shown). Some members have downward vertical velocities that exceed −15 m s^{-1} in the rear of the hook echo (e.g., Fig. 7k), while others have more subdued signals of descent (e.g., Fig. 7l). *Considering the differences in*

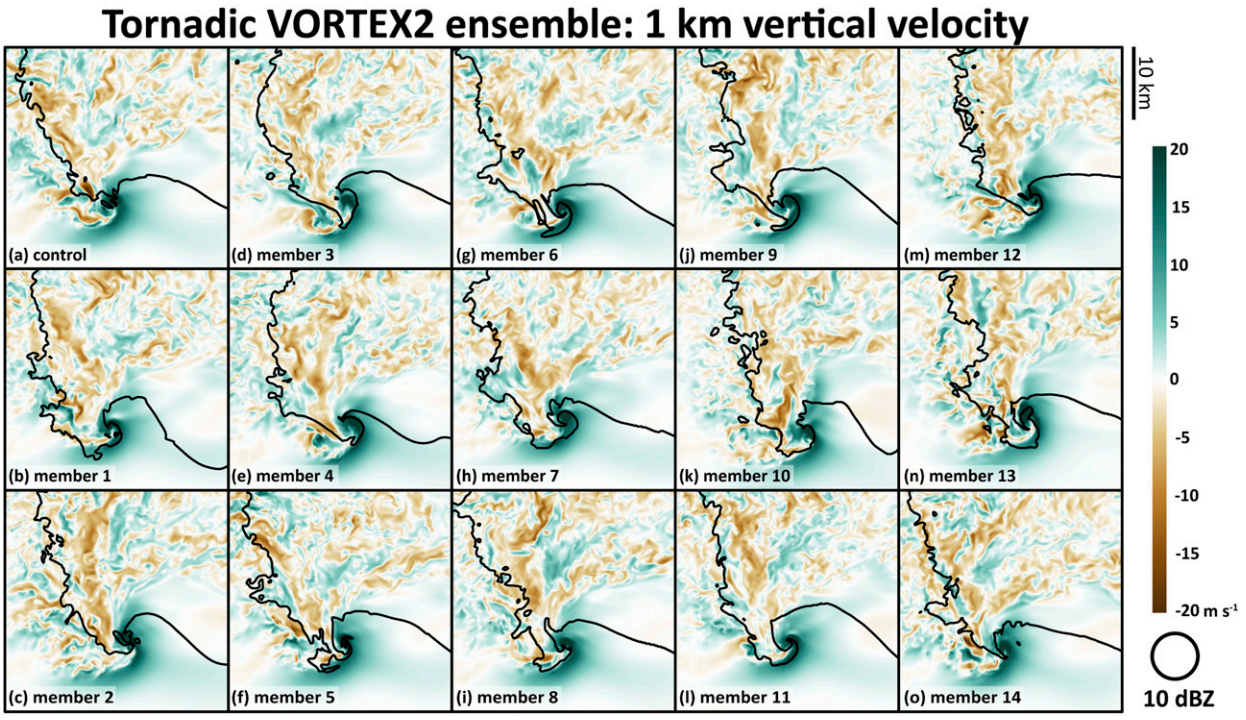

FIG. 7. Horizontal cross sections of 1 km AGL vertical velocity (m s^{-1}; shaded) at the key time period of tornadogenesis for the tornadic VORTEX2 ensemble. The 10-dBZ reflectivity contour (black) at 10 m AGL for the respective ensemble members is shown for reference (refer to Fig. 3 for each ensemble member's key time index).

the downdrafts and lower-tropospheric buoyancy field between the tornadic VORTEX2 ensemble members, it is rather remarkable that each simulation within the tornadic VORTEX2 ensemble produces an intense tornado.

Additional comparisons (not shown) reveal that differences in the ensemble are not primarily due to timing differences between the supercells, indicating the ensemble does indeed contain a range of different storms in similar environments (a major goal of this study); however, there appears to be something fundamental about the VORTEX2 tornadic composite environment that heavily favors tornadic supercells, perhaps the highly streamwise lower-tropospheric horizontal vorticity that induces a steady low-level mesocyclone in each supercell (e.g., as demonstrated by CP17).

Although there are notable differences in the distribution of the precipitation, intensity, and location of downdrafts, as well as the magnitude of near-surface buoyancy within each storm, there are not many differences in the low-level updraft within the ensemble. Indeed, a broad area of strong upward motion at 1 km AGL exists directly above the tip of the hook echo in each member (Fig. 7). The low-level updrafts are also vertically stacked underneath the midlevel updrafts, above the intersection of the rear- and forward-flank outflow boundaries (not shown). Additionally, as in CP17, the low-level updrafts are highly correlated with upward dynamic accelerations in the vicinity of the low-level mesocyclone because of the vertical gradient in the dynamic pressure perturbations (Fig. 8). In each member, the updraft and mesocyclone undergo significant strengthening during the 10 min prior to tornadogenesis. At the time of tornadogenesis, the maximum updraft at 1 km AGL in each member ranges from approximately 30 to 55 m s^{-1} (not shown). In addition to being intense, the updraft is also exceptionally steady, a configuration that CP17 found to be favorable for tornadogenesis in the VORTEX2 composite environments. As demonstrated in CP17, the steady nature of the low-level updraft was directly attributable to the influx of highly streamwise horizontal vorticity into the low-level mesocyclone. Recently, Orf et al. (2017) also showed similar favorable and steady updraft structures were caused by large near-surface streamwise horizontal vorticity (in their case, the ''streamwise vorticity current'' was baroclinically enhanced by the forward-flank outflow).

For all members, circulation C was computed within a 1-km-radius horizontal ring centered at each grid point within the domain's constant grid-spacing inner mesh, using the area (A) sum of vertical vorticity ζ (i.e., $\int_A \zeta \, dA$). The circulation at 1 km AGL in all the tornadic members was considerably higher than the circulation at the surface

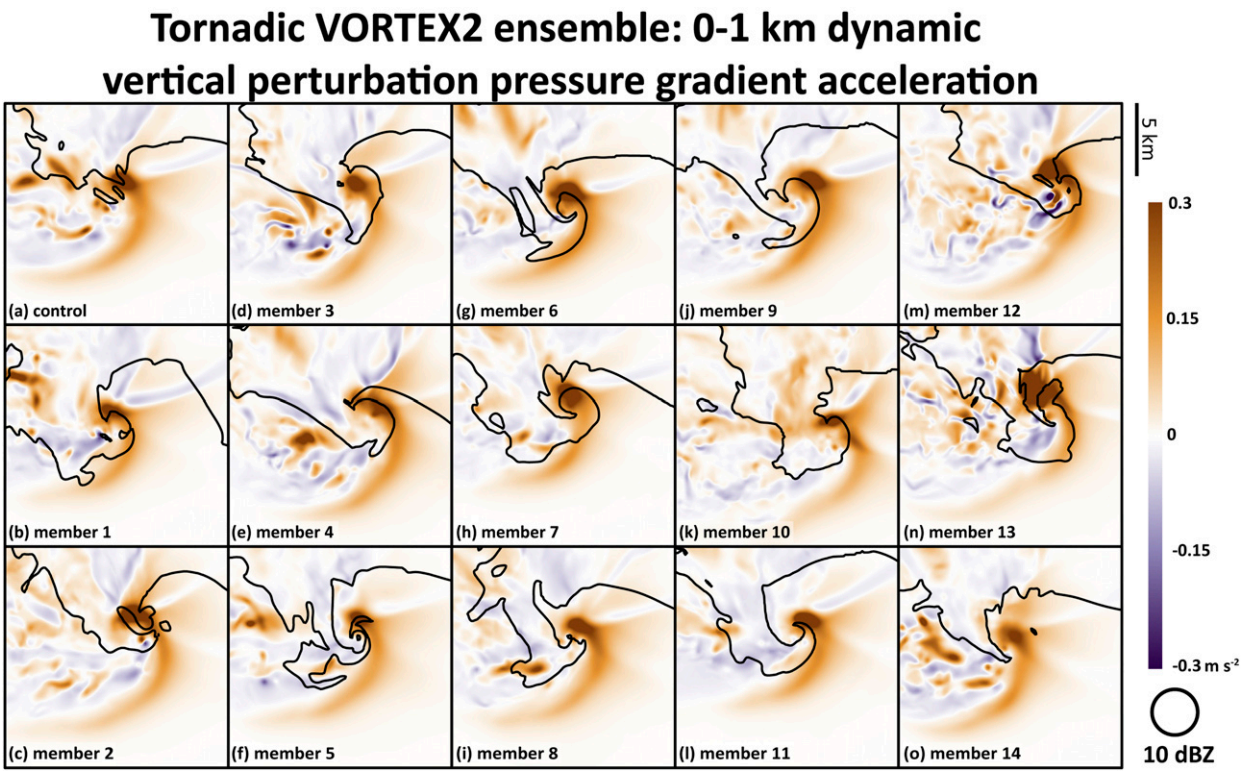

FIG. 8. Horizontal cross sections of 0–1 km AGL dynamic vertical perturbation pressure gradient acceleration ($m\,s^{-2}$; shaded) at the key time period of tornadogenesis for the tornadic VORTEX2 ensemble. The 10-dBZ reflectivity contour (black) at 10 m AGL for the respective ensemble members is shown for reference (refer to Fig. 3 for each ensemble member's key time index).

(Figs. 9a–c). Since circulation is qualitatively related to dynamic pressure minima in flow regimes where the rotation predominates, this indicates that the low-level mesocyclone is set up favorably for upward dynamic accelerations in each of the tornadic VORTEX2 ensemble members (as described in more detail by CP17). Although not presented for each simulation, the low-level circulation at 1 km AGL is highly correlated with the low-level updraft for all members in the tornadic VORTEX2 ensemble (see Fig. 19 in CP17), which is a robust indicator of predominately streamwise horizontal vorticity being ingested into the supercell's low-level mesocyclone (Davies-Jones 1984; CP17).

In summary, the perturbations added to the VORTEX2 tornadic composite wind profile produced 15 distinct supercells, and yet all of them were tornadic. While there are notable differences among the simulations, one main pathway of tornadogenesis occurs: a concentrated area of surface vertical vorticity is converged and stretched underneath an intensifying low-level mesocyclone. The steady, persistent area of strong upward dynamic lifting is due to the ingestion of predominately streamwise horizontal vorticity into the low-level mesocyclone (as in CP17).

b. *Characteristics of the nontornadic VORTEX2 ensemble*

While one main pathway of tornadogenesis occurred in each of the tornadic VORTEX2 ensemble simulations, the nontornadic VORTEX2 ensemble resists generalization. Using the combined tornadogenesis definitions in section 2, 40% of the nontornadic ensemble are considered to be tornadic (members 1, 3, 7, 10, 11, and 12), although it is possible weaker, smaller-scale tornadic processes are not resolved on the 125-m grid. The key time periods of tornadogenesis or tornadogenesis failure range from $t = 62$ to 114 min (Fig. 10), with the maximum surface vertical vorticity for each member ranging from 0.32 to $0.88\,s^{-1}$. Only one member (member 3) has a maximum surface vertical vorticity ($0.88\,s^{-1}$) that falls within the range of the tornadic VORTEX2 ensemble, a value comparable to the weakest of the tornadic VORTEX2 ensemble (member 10). Member 10 in the tornadic VORTEX2 ensemble is still clearly more intense than any of the nontornadic VORTEX2 ensemble members (not shown).

The supercells in members 7, 10, and 12 (Figs. 11h,k,m) are considered to be "weakly tornadic" [arbitrarily defined

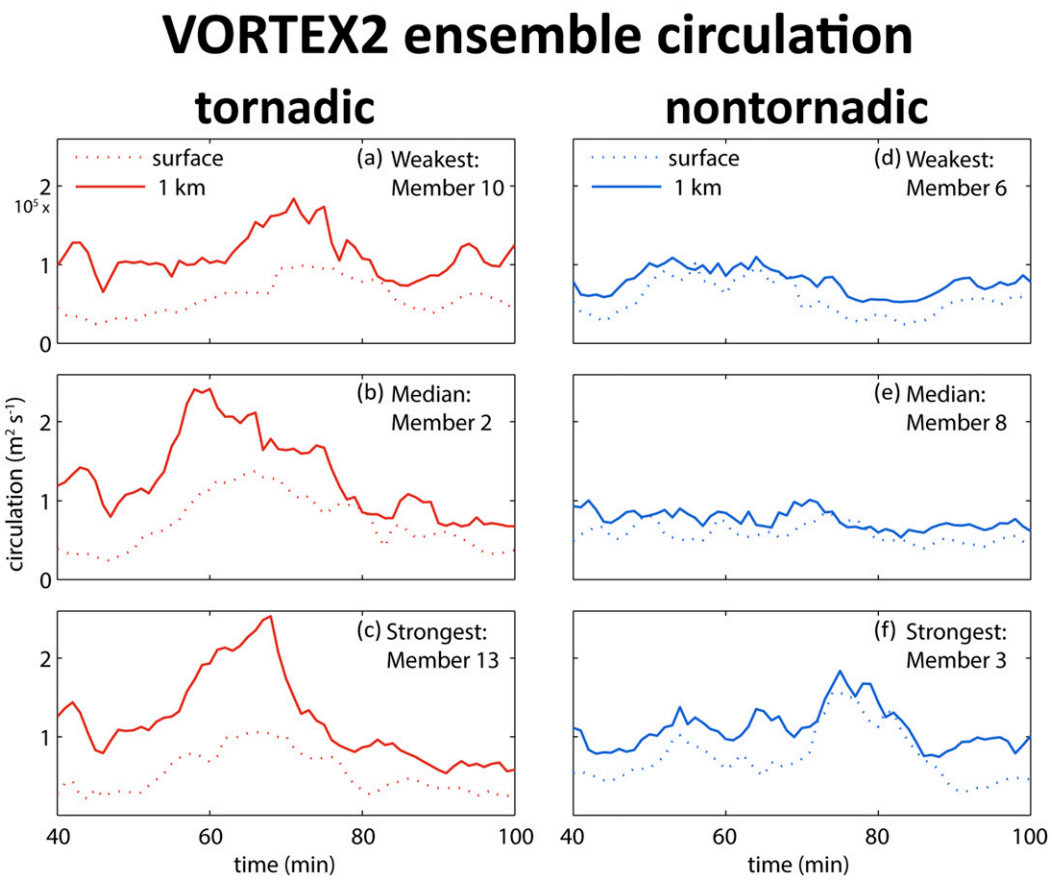

FIG. 9. Time series comparing the maximum circulation ($m^2 s^{-1}$) for both the (a)–(c) tornadic (red) and (d)–(f) nontornadic (blue) VORTEX2 ensembles. The (top) weakest, (middle) median, and (bottom) strongest members based on maximum surface vertical vorticity are shown for each ensemble. Circulation was computed around a 1-km-radius horizontal ring centered at each grid point at the surface (dotted line) and at 1 km AGL (solid line) for each ensemble member.

as a tornadic supercell that produces an EF0–EF1 tornado for ≤5 min, as in Markowski et al. (2002)]. These supercells only briefly produce vortices that meet the minimum requirements of tornadogenesis outlined in section 2. While they produce higher values of vertical vorticity ($\geq 0.4\,s^{-1}$) than the other nontornadic VORTEX2 ensemble members, the vortices are brief, transient spinups that last only a couple of minutes and do not exhibit the characteristic surface vertical vorticity swaths that the other tornadic members in both the nontornadic and tornadic VORTEX2 ensembles do (cf. Figs. 11h,k,m with Figs. 11b,d,l and each member in Fig. 4). The wind speeds in these vortices never exceed the EF1 wind speed threshold, and they also critically lack significant pressure deficits (<−20 hPa), both at the surface and throughout the lower troposphere, compared to the other tornadic members.

Of the six tornadic supercells in the nontornadic VORTEX2 ensemble, only the strongest three (20%; members 1, 3, and 11) have the consistent tornadic signatures of sustained, vertically continuous vertical vorticity and pressure deficits as in the tornadic VORTEX2 ensemble. Unlike the weakly tornadic supercells, members 1, 3, and 11 (Figs. 11b,d,l) produce surface vertical vorticity swaths that exceed $0.3\,s^{-1}$ for approximately 10 km and last 5–10 min. Albeit undoubtedly weaker than the tornadic VORTEX2 ensemble, they exhibit deep pressure falls (<−20 hPa) throughout the lower troposphere (not shown). However, as will be shown below, it is not obvious from the reflectivity, surface vertical vorticity, near-surface buoyancy, or the low-level updraft why these seemingly similar storms in the nontornadic VORTEX2 ensemble produced tornadoes while the rest of the ensemble did not.

At no point in the nontornadic VORTEX2 ensemble simulations do the supercells appear to be as steady and organized as any of the members in the tornadic VORTEX2 ensemble. Every member has a low-level hook

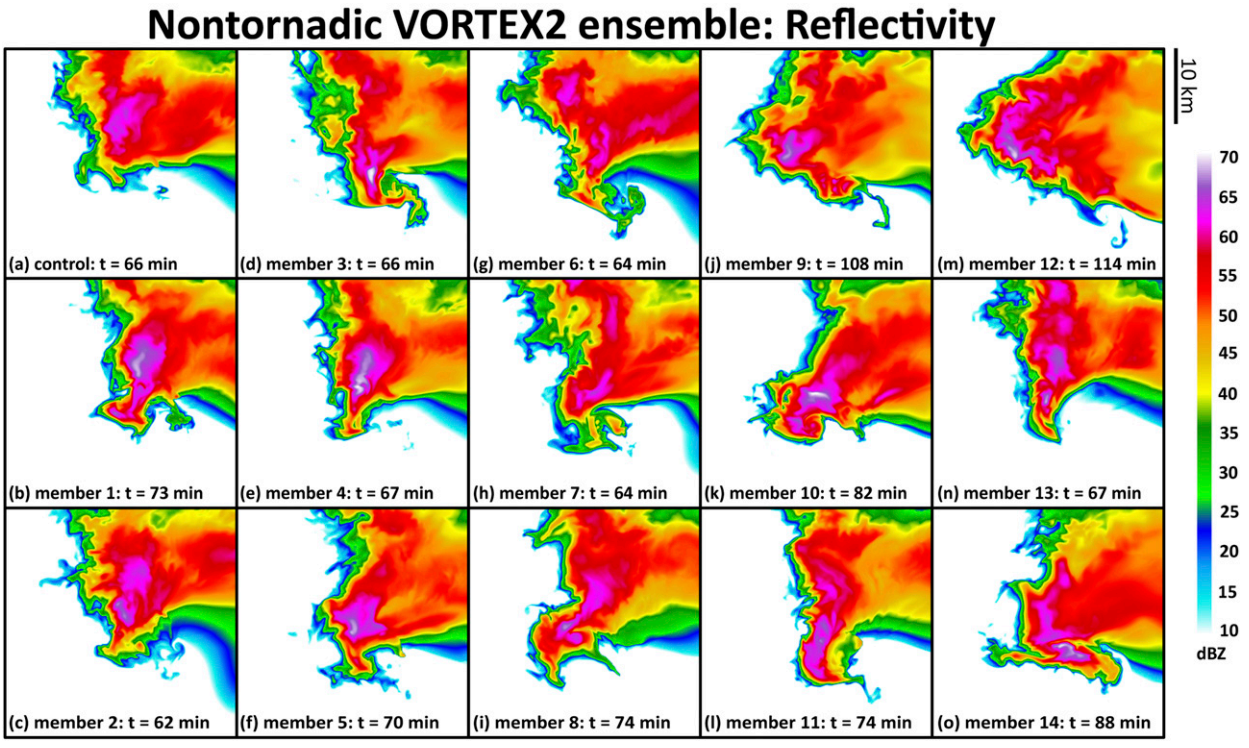

FIG. 10. As in Fig. 3, but for the nontornadic VORTEX2 ensemble.

echo (Fig. 10) and plenty of subtornadic surface vertical vorticity (Fig. 12). Frequent cycling of low-level mesocyclones and attendant hook echoes is often present in the simulations (e.g., Figs. 10b,i,k), with tornadogenesis or tornadogenesis failure in these instances commonly occurring within the rearward hook echo, once the surface circulation is far removed from the main low-level updraft. It is not obvious from the reflectivity field alone which members would be tornadic. Those that are tornadic do not have more distinct hook echoes or more classic supercellular structures (e.g., low- and high-precipitation supercells are commonly considered less likely to be tornadic; Moller et al. 1994). For example, member 3 (Fig. 10d) and member 6 (Fig. 10g) have similar amounts of precipitation within the hook echoes; however, member 3 is tornadic while member 6 is not. Even though the same magnitude of wind perturbations is applied to each ensemble, there is something about the nontornadic VORTEX2 environment that engenders more spread in reflectivity structures within the ensemble compared to the tornadic VORTEX2 ensemble.

The details of the near-surface cold pool structures vary widely between the ensemble members (Fig. 13); however, none of the members is characterized by particularly cold air throughout the hook-echo region, which is known to be unfavorable for tornadoes (see Fig. 14 in Markowski et al. 2002; Grzych et al. 2007). The maximum deficits of the density potential temperature within a 2-km radius of the main surface vortex in each simulation range from −1 to −7 K. For example, member 12 is quite warm (Fig. 13m) while member 10 is rather colder (Fig. 13k), even though both are associated with weak tornadoes. The range of outflow temperatures in the nontornadic VORTEX2 ensemble is quite similar to that of the tornadic VORTEX2 ensemble at tornadogenesis. This is consistent with both ensembles having lifted condensation levels (LCLs; 1129 vs 845 m for the nontornadic and tornadic VORTEX2 profiles, respectively) in the range of significantly tornadic supercells (Thompson et al. 2012).

The tornadic members of the nontornadic VORTEX2 ensemble tend to have minimum density potential temperature deficits at the warmer end of the ensemble's distribution; however, other nontornadic members also have similar outflow deficits (Fig. 13). Thus, relatively small negative buoyancy in the outflow is a necessary but insufficient condition for tornadogenesis in the nontornadic VORTEX2 ensemble [as suggested by Markowski and Richardson (2014)]. The cold pool differences are a result of differences in the location, orientation, and magnitude of downdraft regions between the ensemble members (Fig. 14). Regardless, the main 1 km AGL downdrafts in the nontornadic VORTEX2 ensemble are not noticeably stronger than in the tornadic VORTEX2 ensemble (cf.

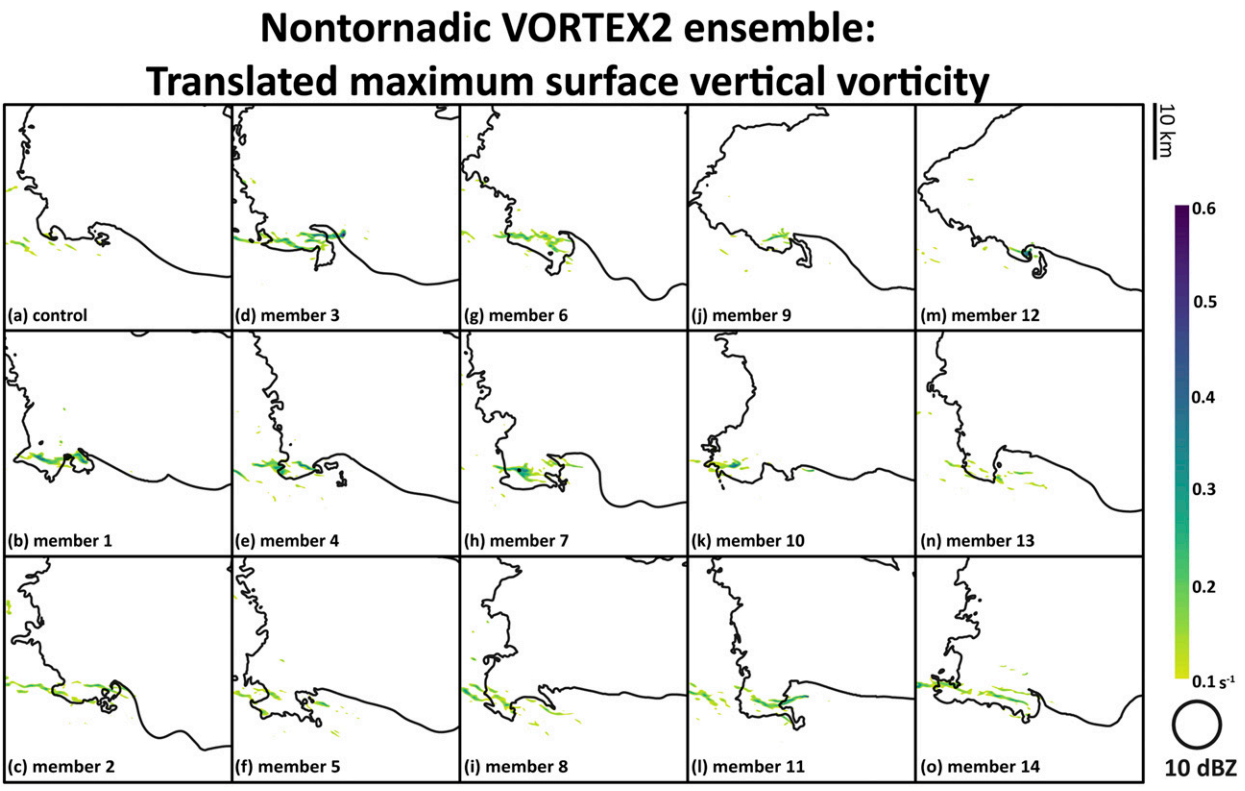

FIG. 11. As in Fig. 4, but for the nontornadic VORTEX2 ensemble. The 10-dBZ reflectivity contour (black) at 10 m AGL is shown for the respective ensemble members at the key time period of tornadogenesis or tornadogenesis failure for the respective ensemble members (refer to Fig. 10 for each ensemble member's key time index).

Figs. 7 and 14), and there is no correlation between downdraft intensity and tornadogenesis (not shown).

Although very cold outflow is an obvious hindrance to tornadogenesis, clearly this may not be the failure mode in some supercells, as intense supercells possessing only moderately negatively buoyant air and ample subtornadic surface vertical vorticity can still sometimes be nontornadic. Additionally, all 15 supercells, regardless of whether they are tornadic or not, had internal surges in the rear-flank outflow near the period of tornadogenesis/failure (not shown), indicating that surges are not exclusive to tornadic supercells. There must be some other explanation for tornadogenesis failure in these supercells.

Despite the outflow in the nontornadic VORTEX2 simulations displaying no obvious signs that would seemingly inhibit tornadogenesis in most of the members, the nontornadic VORTEX2 ensemble predominately produces weak swaths of vertical vorticity (Fig. 11). Typical members have shallow, transient vortices that only persist for a couple of minutes, never reaching the tornadic threshold (e.g., Figs. 11c,e,f,i,j,o), while a couple members produce almost no swaths of large vertical vorticity (e.g., Figs. 11a,n), despite the presence of subtornadic vertical vorticity ($\geq 0.01\,s^{-1}$ at the surface) within the hook-echo region of each ensemble member (Figs. 12a,n). This illustrates a crucial point: *it is not whether a supercell produces surface vertical vorticity that determines if it is tornadic or not, but rather how the ample subtornadic surface vertical vorticity present in all surface-based supercells is converged and stretched by the low-level updraft.*

While the tornadic VORTEX2 ensemble had a consistent updraft signature favorable for tornadogenesis, the nontornadic VORTEX2 ensemble has much more variance in the low-level updraft structure and intensity (Fig. 14). Nevertheless, a fundamental theme emerges: the main updraft is often bowed out along the rear-flank outflow, and behind this, the updraft is notably unsteady with large pockets of descent present in the weak-echo region, consistent with the baseline nontornadic simulation of CP17. This unsteadiness is more relevant than the instantaneous peak values of vertical velocity, as the members with stronger low-level updrafts were not necessarily the ones that produced tornadoes (not shown). Both positive and negative areas of dynamic acceleration frequently form and dissipate overhead of the existing surface vertical vorticity (Fig. 15). Without a persistent area of upward lifting, the surface vertical vorticity that does develop in the

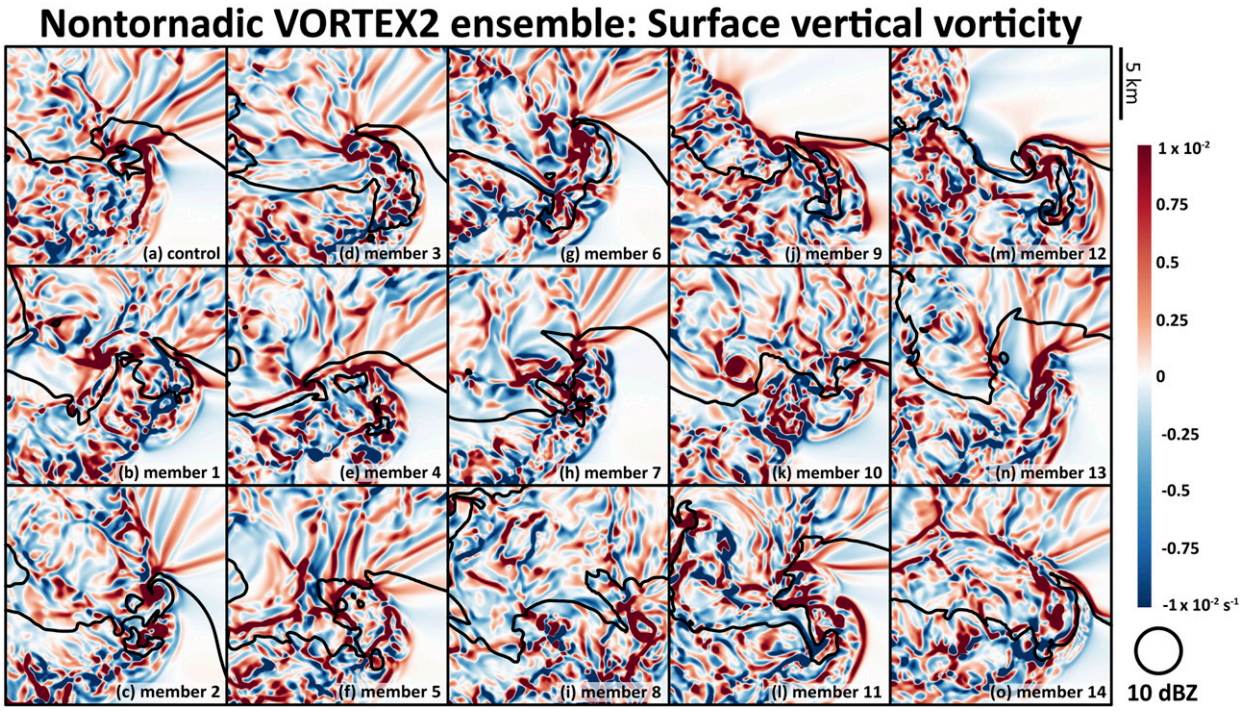

FIG. 12. As in Fig. 6, but for the nontornadic VORTEX2 ensemble. The 10-dBZ reflectivity contour (black) at 10 m AGL is shown for the respective ensemble members at the key time period of tornadogenesis or tornadogenesis failure for the respective ensemble members (refer to Fig. 10 for each ensemble member's key time index).

nontornadic supercells is not likely to be contracted into a tornado. The dynamic accelerations in the tornadic VORTEX2 ensemble members are noticeably stronger in magnitude and universally more organized than the nontornadic VORTEX2 ensemble (cf. Figs. 8 and 15, specifically the large, coherent area of upward accelerations in Fig. 8), even in the members that are marginally tornadic. As shown in CP17, the strikingly disorganized low-level updrafts in the nontornadic VORTEX2 ensemble (compared to the steady low-level updrafts in the tornadic VORTEX2 ensemble) are most likely due to the flux of predominately crosswise horizontal vorticity into the low-level mesocyclone from the nontornadic VORTEX2 wind profile (as shown in more detail by CP17).

In a similar manner to the tornadic VORTEX2 ensemble and the baseline simulations in CP17, the circulation field helps elucidate why the nontornadic VORTEX2 ensemble fails to establish steady low-level dynamic lifting favorable for tornadogenesis. In each nontornadic VORTEX2 ensemble member, surface circulation that is comparable to the tornadic VORTEX2 ensemble members exists, meaning these supercells at least have the potential to become tornadic in the nontornadic environments (Fig. 9). However, the surface circulation is most commonly of equal magnitude to the 1-km circulation (Figs. 9d–f), leading to a lack of a upward-directed dynamic vertical perturbation pressure gradient acceleration to stretch subtornadic vertical vorticity into tornadic strength (Fig. 15). Only in the strongest three members in the nontornadic VORTEX2 ensemble does the circulation exhibit the classic pattern associated with tornadogenesis in CP17 and the tornadic VORTEX2 ensemble herein, where the 1-km circulation strengthens concurrently with the surface circulation (e.g., Figs. 9a–c,f). Yet, even when this occurs in the nontornadic VORTEX2 ensemble, the surface circulation is nearly of equal magnitude to the 1-km circulation (Fig. 9f), indicating the potential for dynamically induced downdrafts that disrupt the formation of developing vortices (Fig. 15). While it is not possible to present each individual simulation here, an examination of all 15 supercells reveals that the orientation of circulation at 1 km AGL is configured as a cyclonic–anticyclonic couplet located primarily behind the main updraft region and is associated with a deformational wind field, rather than a closed circulation (see Fig. 18 in CP17). Since deformation is associated with locally positive dynamic pressure perturbations (Markowski and Richardson 2010, 28–30), there are commonly positive nonlinear dynamic pressure perturbations at 1 km AGL in the nontornadic VORTEX2 ensemble, even in

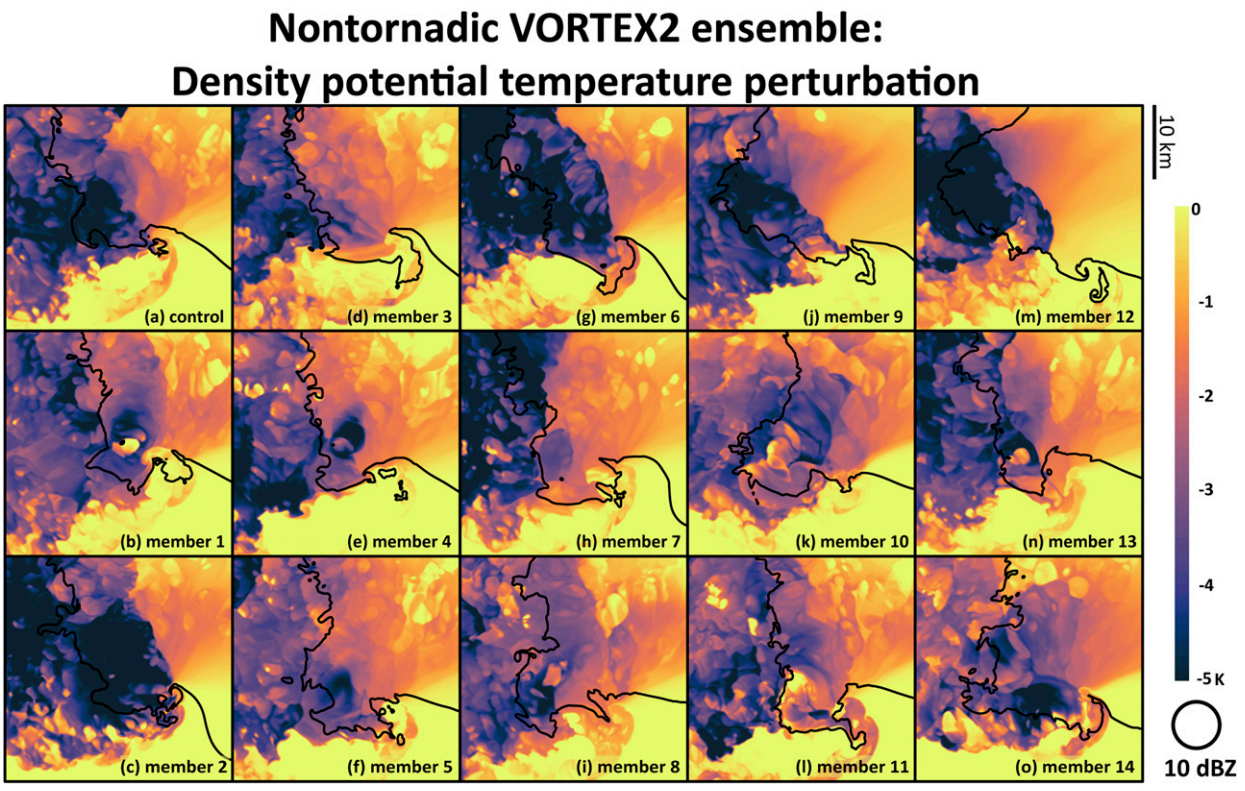

FIG. 13. As in Fig. 5, but for the nontornadic VORTEX2 ensemble. The 10-dB*Z* reflectivity contour (black) at 10 m AGL at the key time period of tornadogenesis or tornadogenesis failure for the respective ensemble members is shown for reference (refer to Fig. 10 for each ensemble member's key time index).

the simulations that are tornadic. The positive–negative circulation couplet straddling the updraft is a robust indicator of the tilting and advection of crosswise horizontal vorticity by the storm-relative wind into a supercell's updraft (Davies-Jones 1984; CP17).

In summary, despite identical perturbations to the wind profile between the nontornadic and tornadic VORTEX2 ensembles, the nontornadic VORTEX2 ensemble results in a greater variation in solutions than the tornadic VORTEX2 ensemble. Twenty percent of the simulations in the nontornadic VORTEX2 ensemble produce supercells that are tornadic, although each of these is clearly weaker than any of the tornadoes from the tornadic VORTEX2 ensemble. An additional 20% of the nontornadic VORTEX2 ensemble is marginally tornadic, producing vortices that meet the tornadic criteria but only transiently. Each nontornadic VORTEX2 simulation features a supercell with a disorganized low-level mesocyclone, with minimal significant dynamic pressure falls at 1 km AGL. This leads to insufficient dynamic lifting and stretching of parcels that acquire surface vertical vorticity within the nontornadic supercells. The disorganized low-level mesocyclone and lack of dynamic lifting appears to be linked to predominately crosswise vorticity in the lowest few hundred meters in the nontornadic environment, just as in the baseline nontornadic simulation of CP17.

4. Synthesis

a. Summary

In this article, we investigated the impact of relatively minor variations in the environmental wind profile upon the range of tornadogenesis outcomes in an ensemble of supercell storms. Despite an increased understanding of the environmental controls on tornado formation in recent years, a high false-alarm rate for tornado warnings still exists, perhaps because of the possibility that tornado formation could be a volatile, stochastic process internal to each storm. This may result in a wide range of outcomes for supercells, even in environments known to be favorable (or unfavorable) for tornadoes. Our previous study indicated that key differences in the lower-tropospheric wind profile in the VORTEX2 composite environmental profiles, specifically the orientation of the horizontal vorticity in the lowest few hundred

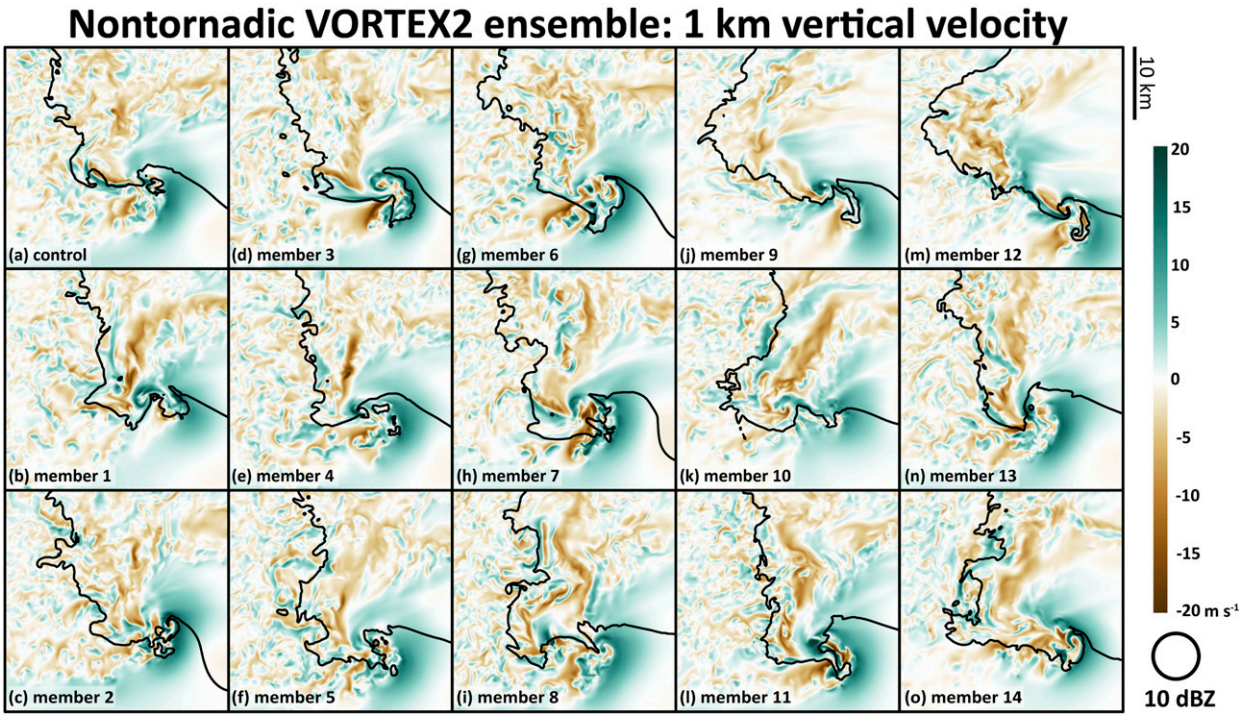

FIG. 14. As in Fig. 7, but for the nontornadic VORTEX2 ensemble. The 10-dB*Z* reflectivity contour (black) at 10 m AGL at the key time period of tornadogenesis or tornadogenesis failure for the respective ensemble members is shown for reference (refer to Fig. 10 for each ensemble member's key time index).

meters AGL, were ultimately determinative of a storm's tornadic potential. However, we were concerned that those results might have been serendipitous (i.e., that the nontornadic and tornadic environments produced the "correct outcome" by chance). The ensemble simulations herein help to quantify the role of the environment versus the possibly stochastic nature of within-storm fluctuations. Our main conclusions are as follows:

- Even though the ensemble is initialized with only minor variations to the VORTEX2 nontornadic and tornadic composite environmental profiles, the perturbations are quite impactful to the resulting precipitation and cold pool structures. Differences in each ensemble do not appear to be solely due to temporal phasing differences between the supercells. The ensemble supports the idea that a range of distinctly different storms can occur in very similar environments.
- Each of the 15 members in the tornadic VORTEX2 ensemble produced long-track intense tornadoes, resulting in a neighborhood probability of tornadic-strength vertical vorticity greater than 95% within the ensemble (despite spatial displacements; Fig. 16a). Although there are notable differences in the distribution of precipitation, intensity and location of downdrafts, and the magnitude of near-surface buoyancy, these differences are not determining factors in whether or not a tornado forms. Instead, the most important component of the simulations is that each storm features a steady low-level mesocyclone due to the ingestion of predominately streamwise horizontal vorticity. This configuration of the low-level mesocyclone provides a persistent area of strong upward dynamic lifting to contract and stretch subtornadic surface vertical vorticity into a tornado. This fundamental attribute of the VORTEX2 tornadic composite environment (highly streamwise lower-tropospheric horizontal vorticity) seems to strongly favor tornadic supercells.
- Forty percent of the ensemble members initialized with the nontornadic VORTEX2 profile are actually tornadic, with half of those only being weakly tornadic (EF0–EF1 tornado for $\leq$5 min). The neighborhood probability of a tornado within the ensemble is much lower than the tornadic VORTEX2 ensemble but crucially is nonzero (peaking near 35%; Fig. 16b). It is not obvious from the reflectivity, surface vertical vorticity, near-surface buoyancy, or the low-level updraft, why these seemingly similar storms in the nontornadic VORTEX2 ensemble produced tornadoes while the rest of the ensemble did not. Even though six members of the nontornadic VORTEX2 ensemble produced a tornado, each of the vortices was unquestionably weaker than any

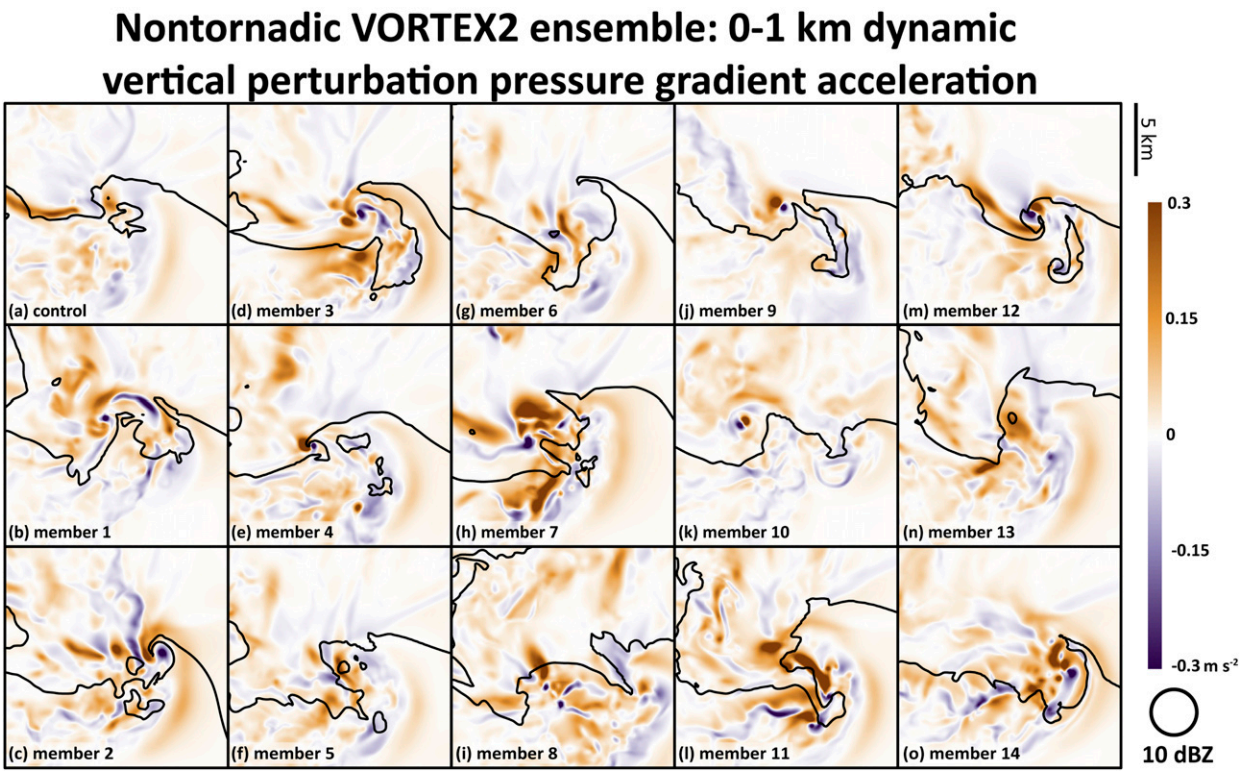

FIG. 15. As in Fig. 8, but for the nontornadic VORTEX2 ensemble. The 10-dB*Z* reflectivity contour (black) at 10 m AGL at the key time period of tornadogenesis or tornadogenesis failure for the respective ensemble members is shown for reference (refer to Fig. 10 for each ensemble member's key time index).

of the tornadic VORTEX2 ensemble members, although it is possible smaller-scale tornadic processes are not resolved with the current grid spacing. This implies that, even though chaotic within-storm details can occasionally lead to marginally tornadic vortices, these vortices are still a weaker class than the tornadic vortices produced by supercells in more favorable environments.

- Each nontornadic VORTEX2 simulation features a supercell with a disorganized low-level mesocyclone, with no significant dynamic pressure falls at 1 km AGL. This leads to insufficient dynamic lifting and stretching of parcels that acquire surface vertical vorticity within the nontornadic supercells. The disorganized low-level mesocyclone and lack of dynamic lifting appear to be linked to predominately crosswise vorticity in the lowest few hundred meters in the nontornadic environment, just as in the baseline nontornadic simulation of CP17.

b. *Discussion and future work*

A key, emerging theme from these and other recent simulations (e.g., Parker and Dahl 2015, CP17) is that it ostensibly does not matter how a supercell generates near-ground rotation (whether via barotropic, baroclinic, or frictional processes). Rather, it is more practically pertinent to ascertain whether (and how) the ample near-surface rotation present in all surface-based supercells is converged and stretched by the low-level updraft into a tornadic-strength vortex (i.e., the third and final step of the tornadogenesis process; Davies-Jones 2015). Fortunately, for operational forecasting purposes, the eventual fate of subtornadic surface vertical vorticity is not determined solely by the cold pool buoyancy, but rather that tornadogenesis seems to be substantially modulated by the environmental wind profile (at least for the VORTEX2 composite environments), even as chaotic within-storm details still permit a range of possible outcomes (as in the nontornadic VORTEX2 ensemble). This is encouraging operationally because lower-tropospheric SRH can be diagnosed more easily than outflow buoyancy.

The focus of the ensemble simulations herein and the baseline nontornadic and tornadic simulations in CP17 has been on the orientation of the lower-tropospheric horizontal vorticity because high SRH favors a stronger low-level mesocyclone and thus greater dynamic lifting (e.g., Markowski and Richardson 2014). Perhaps large streamwise horizontal vorticity in the lower troposphere, and the resulting steady, intense low-level mesocyclones

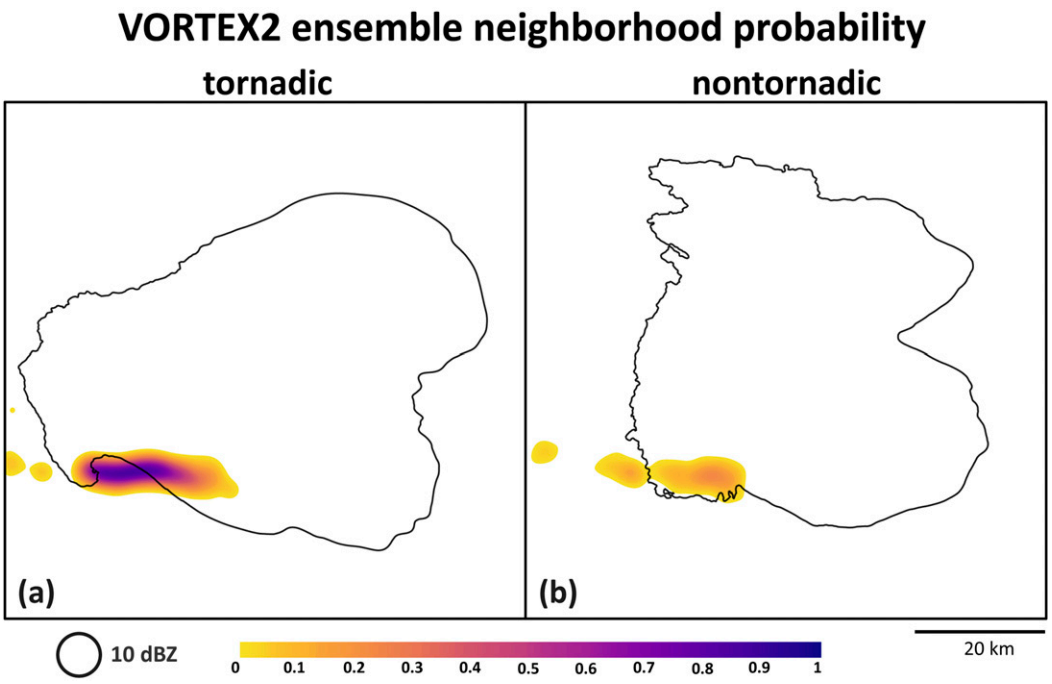

FIG. 16. Neighborhood probability (shaded) of 10 m AGL translated maximum vertical vorticity exceeding a threshold of 0.3 s^{-1} from Figs. 4 and 11 anywhere within the neighborhood during a 45-min time period surrounding the key time period of tornadogenesis or tornadogenesis failure for each ensemble member (10 min before, 35 min after) for both the (a) tornadic and (b) nontornadic VORTEX2 ensembles. The neighborhood consisted of 12 points (1.5 km). Additionally, a Gaussian smoother is applied with a standard deviation of 1.5 km. The composite 10-dBZ reflectivity contour (black) at 10 m AGL at the key time period of tornadogenesis or tornadogenesis failure for the respective ensemble is shown for reference. See Schwartz and Sobash (2017) for more information on probabilistic neighborhood approaches.

(as in the tornadic VORTEX2 ensemble), are why on some rare days nearly every storm is tornadic despite variations in the near-surface buoyancy field [a conundrum highlighted by Markowski and Richardson (2017)]. Unfortunately, the present simulations fail to completely address why environments that seem to be very supportive for tornadogenesis sometimes fail to yield tornadoes (i.e., all of our tornadic ensemble members produced tornadoes). Our knowledge of the environmental controls on tornado formation is almost certainly still incomplete [as suggested by Anderson-Frey et al. (2016)]. Perhaps, since the ingestion of crosswise horizontal vorticity influences the organization of the low-level mesocyclone, the tornadic potential of environments could be discriminated through a ratio of streamwise to crosswise horizontal vorticity, instead of solely just SRH. After all, high SRH is commonly achievable when the lower-tropospheric environmental vertical wind shear vector magnitude is large, even when the orientation of lower-tropospheric horizontal vorticity is predominately crosswise.

Since the values of 0–1-km and effective SRH within both ensembles (Table 2) are generally considered favorable for tornadoes (e.g., Thompson et al. 2007), maybe it is not surprising that as much as 40% of the nontornadic VORTEX2 ensemble would be tornadic (albeit weaker than the tornadic VORTEX2 ensemble). However, one of the biggest distinctions between the VORTEX2 composite environments was the 0–500-m SRH. CP17 found parcels in this layer were crucially important to the eventual characteristics of the low-level mesocyclone and ultimately tornadogenesis versus failure. It is possible that looking at shallower layers of SRH than are conventionally used operationally, in addition to both the streamwise and crosswise components of horizontal vorticity, will lead to clearer boundaries between environments of nontornadic and significantly tornadic supercells. Future work will explore these possibilities through observations and simulations.

The current range of 0–500-m SRH (60–96 and 138–174 $m^2 s^{-2}$ for the nontornadic and tornadic environments, respectively; Table 2) produced by the random wind perturbations does not result in a ''tipping point'' between nontornadic and tornadic supercells. In fact, there is no correlation between the 0–500-m SRH and maximum surface vertical vorticity within either the

nontornadic or tornadic VORTEX2 ensemble (not shown). This suggests that, if there is a critical value of lower-tropospheric streamwise horizontal vorticity that heavily favors tornadic supercells, the current nontornadic VORTEX2 ensemble does not reach that threshold. Furthermore, considering that all members of the tornadic VORTEX2 ensemble produce a tornado, it is unclear what amount of near-surface crosswise horizontal vorticity is necessary to disrupt the low-level mesocyclone sufficiently for tornadogenesis failure. Therefore, additional simulations with interpolated wind profiles between the nontornadic and tornadic VORTEX2 environments are currently ongoing to address this research question.

Ultimately, an understanding of how environmental ingredients link to the predictability of tornadic versus nontornadic storms will require studies that span a much broader range of the supercell spectrum than what is represented by the VORTEX2 composite environments. Future work will investigate tornadogenesis failure in more diverse environments (e.g., event and null cases from VORTEX2 and VORTEX-Southeast), as well as more varied ways to add spread to the ensemble (thermodynamic perturbations, microphysics, etc.). We view the present methods as a promising first step toward isolating the part of the problem that is specifically due to within-storm variability.

Acknowledgments. This research was supported by NSF Grant AGS-1156123 and NOAA Grants NA15OAR4590235 and NA16OAR4590213. We would like to acknowledge high-performance computing support from Yellowstone (ark:/85065/d7wd3xhc) provided by NCAR's Computational and Information Systems Laboratory, sponsored by the National Science Foundation. We especially thank Dr. George Bryan for his ongoing support of CM1. We also thank the three anonymous reviewers who provided invaluable feedback on this article. Members of the BEC's committee, Drs. Gary Lackmann and Sandra Yuter, as well as members of the NCSU Convective Storms group (Andy Wade, Brett Borchardt, Pat Hawbecker, and Keith Sherburn) provided helpful feedback on an earlier version of this manuscript.

REFERENCES

Adlerman, E. J., and K. K. Droegemeier, 2005: The dependence of numerically simulated cyclic mesocyclogenesis upon environmental vertical wind shear. *Mon. Wea. Rev.*, **133**, 3595–3623, doi:10.1175/MWR3039.1.

——, ——, and R. Davies-Jones, 1999: A numerical simulation of cyclic mesocyclogenesis. *J. Atmos. Sci.*, **56**, 2045–2069, doi:10.1175/1520-0469(1999)056<2045:ANSOCM>2.0.CO;2.

Anderson-Frey, A. K., Y. P. Richardson, A. R. Dean, R. L. Thompson, and B. T. Smith, 2016: Investigation of near-storm environments for tornado events and warnings. *Wea. Forecasting*, **31**, 1771–1790, doi:10.1175/WAF-D-16-0046.1.

Brooks, H. E., 2004a: On the relationship of tornado path length and width to intensity. *Wea. Forecasting*, **19**, 310–319, doi:10.1175/1520-0434(2004)019<0310:OTROTP>2.0.CO;2.

——, 2004b: Tornado-warning performance in the past and future: A perspective from signal detection theory. *Bull. Amer. Meteor. Soc.*, **85**, 837–843, doi:10.1175/BAMS-85-6-837.

Brotzge, J., S. Erickson, and H. Brooks, 2011: A 5-yr climatology of tornado false alarms. *Wea. Forecasting*, **26**, 534–544, doi:10.1175/WAF-D-10-05004.1.

Bryan, G. H., and H. Morrison, 2012: Sensitivity of a simulated squall line to horizontal resolution and parameterization of microphysics. *Mon. Wea. Rev.*, **140**, 202–225, doi:10.1175/MWR-D-11-00046.1.

——, J. C. Wyngaard, and J. M. Fritsch, 2003: Resolution requirements for the simulation of deep moist convection. *Mon. Wea. Rev.*, **131**, 2394–2416, doi:10.1175/1520-0493(2003)131<2394:RRFTSO>2.0.CO;2.

Bunkers, M. J., B. A. Klimowski, J. W. Zeitler, R. L. Thompson, and M. L. Weisman, 2000: Predicting supercell motion using a new hodograph technique. *Wea. Forecasting*, **15**, 61–79, doi:10.1175/1520-0434(2000)015<0061:PSMUAN>2.0.CO;2.

Coffer, B. E., and M. D. Parker, 2015: Impacts of increasing low-level shear on supercells during the early evening transition. *Mon. Wea. Rev.*, **143**, 1945–1969, doi:10.1175/MWR-D-14-00328.1.

——, and ——, 2017: Simulated supercells in nontornadic and tornadic VORTEX2 environments. *Mon. Wea. Rev.*, **145**, 149–180, doi:10.1175/MWR-D-16-0226.1.

Dahl, J. M., 2015: Near-ground rotation in simulated supercells: On the robustness of the baroclinic mechanism. *Mon. Wea. Rev.*, **143**, 4929–4942, doi:10.1175/MWR-D-15-0115.1.

——, M. D. Parker, and L. J. Wicker, 2014: Imported and storm-generated near-ground vertical vorticity in a simulated supercell. *J. Atmos. Sci.*, **71**, 3027–3051, doi:10.1175/JAS-D-13-0123.1.

Davies-Jones, R., 1984: Streamwise vorticity: The origin of updraft rotation in supercell storms. *J. Atmos. Sci.*, **41**, 2991–3006, doi:10.1175/1520-0469(1984)041<2991:SVTOOU>2.0.CO;2.

——, 2015: A review of supercell and tornado dynamics. *Atmos. Res.*, **158–159**, 274–291, doi:10.1016/j.atmosres.2014.04.007.

——, and H. Brooks, 1993: Mesocyclogenesis from a theoretical perspective. *The Tornado: Its Structure, Dynamics, Prediction, and Hazards*, *Geophys. Monogr.*, Vol. 79, Amer. Geophys. Union, 105–114.

Dawson, D. T., II, L. J. Wicker, E. R. Mansell, and R. L. Tanamachi, 2012: Impact of the environmental low-level wind profile on ensemble forecasts of the 4 May 2007 Greensburg, Kansas, tornadic storm and associated mesocyclones. *Mon. Wea. Rev.*, **140**, 696–716, doi:10.1175/MWR-D-11-00008.1.

Deardorff, J. W., 1980: Stratocumulus-capped mixed layers derived from a three-dimensional model. *Bound.-Layer Meteor.*, **18**, 495–527, doi:10.1007/BF00119502.

Dowell, D. C., and L. J. Wicker, 2009: Additive noise for storm-scale ensemble data assimilation. *J. Atmos. Oceanic Technol.*, **26**, 911–927, doi:10.1175/2008JTECHA1156.1.

——, ——, and C. Snyder, 2011: Ensemble Kalman filter assimilation of radar observations of the 8 May 2003 Oklahoma City supercell: Influences of reflectivity observations on storm-scale

analyses. *Mon. Wea. Rev.*, **139**, 272–294, doi:10.1175/2010MWR3438.1.

Emanuel, K. A., 1994: *Atmospheric Convection.* Oxford University Press, 592 pp.

Grzych, M. L., B. D. Lee, and C. A. Finley, 2007: Thermodynamic analysis of supercell rear-flank downdrafts from Project ANSWERS. *Mon. Wea. Rev.*, **135**, 240–246, doi:10.1175/MWR3288.1.

Klees, A. M., Y. P. Richardson, P. M. Markowski, C. T. Weiss, J. M. Wurman, and K. Kosiba, 2016: Comparison of the tornadic and nontornadic supercells intercepted by VORTEX2 on 10 June 2010. *Mon. Wea. Rev.*, **144**, 3201–3231, doi:10.1175/MWR-D-15-0345.1.

Klemp, J. B., and R. B. Wilhelmson, 1978: The simulation of three-dimensional convective storm dynamics. *J. Atmos. Sci.*, **35**, 1070–1096, doi:10.1175/1520-0469(1978)035<1070:TSOTDC>2.0.CO;2.

Kosiba, K., J. Wurman, Y. Richardson, P. Markowski, P. Robinson, and J. Marquis, 2013: Genesis of the Goshen County, Wyoming, tornado on 5 June 2009 during VORTEX2. *Mon. Wea. Rev.*, **141**, 1157–1181, doi:10.1175/MWR-D-12-00056.1.

Lee, B. D., C. A. Finley, and C. D. Karstens, 2012: The Bowdle, South Dakota, cyclic tornadic supercell of 22 May 2010: Surface analysis of rear-flank downdraft evolution and multiple internal surges. *Mon. Wea. Rev.*, **140**, 3419–3441, doi:10.1175/MWR-D-11-00351.1.

Mansell, E. R., 2010: On sedimentation and advection in multi-moment bulk microphysics. *J. Atmos. Sci.*, **67**, 3084–3094, doi:10.1175/2010JAS3341.1.

——, C. L. Ziegler, and E. C. Bruning, 2010: Simulated electrification of a small thunderstorm with two-moment bulk microphysics. *J. Atmos. Sci.*, **67**, 171–194, doi:10.1175/2009JAS2965.1.

Markowski, P. M., 2002: Hook echoes and rear-flank downdrafts: A review. *Mon. Wea. Rev.*, **130**, 852–876, doi:10.1175/1520-0493(2002)130<0852:HEARFD>2.0.CO;2.

——, 2016: An idealized numerical simulation investigation of the effects of surface drag on the development of near-surface vorticity in supercell thunderstorms. *J. Atmos. Sci.*, **73**, 4349–4385, doi:10.1175/JAS-D-16-0150.1.

——, and Y. P. Richardson, 2010: *Mesoscale Meteorology in Midlatitudes.* Wiley-Blackwell, 372 pp.

——, and ——, 2014: The influence of environmental low-level shear and cold pools on tornadogenesis: Insights from idealized simulations. *J. Atmos. Sci.*, **71**, 243–275, doi:10.1175/JAS-D-13-0159.1.

——, and ——, 2017: Large sensitivity of near-surface vertical vorticity development to heat sink location in idealized simulations of supercell-like storms. *J. Atmos. Sci.*, **74**, 1095–1104, doi:10.1175/JAS-D-16-0372.1.

——, J. M. Straka, and E. N. Rasmussen, 2002: Direct surface thermodynamic observations within the rear-flank downdrafts of nontornadic and tornadic supercells. *Mon. Wea. Rev.*, **130**, 1692–1721, doi:10.1175/1520-0493(2002)130<1692:DSTOWT>2.0.CO;2.

——, C. Hannon, J. Frame, E. Lancaster, A. Pietrycha, R. Edwards, and R. L. Thompson, 2003: Characteristics of vertical wind profiles near supercells obtained from the Rapid Update Cycle. *Wea. Forecasting*, **18**, 1262–1272, doi:10.1175/1520-0434(2003)018<1262:COVWPN>2.0.CO;2.

——, and Coauthors, 2012a: The pretornadic phase of the Goshen County, Wyoming, supercell of 5 June 2009 intercepted by VORTEX2. Part I: Evolution of kinematic and surface thermodynamic fields. *Mon. Wea. Rev.*, **140**, 2887–2915, doi:10.1175/MWR-D-11-00336.1.

——, and Coauthors, 2012b: The pretornadic phase of the Goshen County, Wyoming, supercell of 5 June 2009 intercepted by VORTEX2. Part II: Intensification of low-level rotation. *Mon. Wea. Rev.*, **140**, 2916–2938, doi:10.1175/MWR-D-11-00337.1.

Marquis, J., Y. Richardson, J. Wurman, and P. Markowski, 2008: Single- and dual-Doppler analysis of a tornadic vortex and surrounding storm-scale flow in the Crowell, Texas, supercell of 30 April 2000. *Mon. Wea. Rev.*, **136**, 5017–5043, doi:10.1175/2008MWR2442.1.

——, ——, P. Markowski, D. Dowell, and J. Wurman, 2012: Tornado maintenance investigated with high-resolution dual-Doppler and EnKF analysis. *Mon. Wea. Rev.*, **140**, 3–27, doi:10.1175/MWR-D-11-00025.1.

Moller, A. R., C. A. Doswell III, M. P. Foster, and G. R. Woodall, 1994: The operational recognition of supercell thunderstorm environments and storm structures. *Wea. Forecasting*, **9**, 327–347, doi:10.1175/1520-0434(1994)009<0327:TOROST>2.0.CO;2.

Naylor, J., and M. S. Gilmore, 2012: Convective initiation in an idealized cloud model using an updraft nudging technique. *Mon. Wea. Rev.*, **140**, 3699–3705, doi:10.1175/MWR-D-12-00163.1.

——, and ——, 2014: Vorticity evolution leading to tornadogenesis and tornadogenesis failure in simulated supercells. *J. Atmos. Sci.*, **71**, 1201–1217, doi:10.1175/JAS-D-13-0219.1.

Orf, L., R. Wilhelmson, B. Lee, C. Finley, and A. Houston, 2017: Evolution of a long-track violent tornado within a simulated supercell. *Bull. Amer. Meteor. Soc.*, **98**, 45–68, doi:10.1175/BAMS-D-15-00073.1.

Parker, M. D., 2014: Composite VORTEX2 supercell environments from near-storm soundings. *Mon. Wea. Rev.*, **142**, 508–529, doi:10.1175/MWR-D-13-00167.1.

——, and J. M. Dahl, 2015: Production of near-surface vertical vorticity by idealized downdrafts. *Mon. Wea. Rev.*, **143**, 2795–2816, doi:10.1175/MWR-D-14-00310.1.

Rotunno, R., and J. Klemp, 1985: On the rotation and propagation of simulated supercell thunderstorms. *J. Atmos. Sci.*, **42**, 271–292, doi:10.1175/1520-0469(1985)042<0271:OTRAPO>2.0.CO;2.

Schenkman, A. D., M. Xue, and D. T. Dawson II, 2016: The cause of internal outflow surges in a high-resolution simulation of the 8 May 2003 Oklahoma City tornadic supercell. *J. Atmos. Sci.*, **73**, 353–370, doi:10.1175/JAS-D-15-0112.1.

Schwartz, C. S., and R. A. Sobash, 2017: Generating probabilistic forecasts from convection-allowing ensembles using neighborhood approaches: A review and recommendations. *Mon. Wea. Rev.*, **145**, 3397–3418, https://doi.org/10.1175/MWR-D-16-0400.1.

Skinner, P. S., C. C. Weiss, M. M. French, H. B. Bluestein, P. M. Markowski, and Y. P. Richardson, 2014: VORTEX2 observations of a low-level mesocyclone with multiple internal rear-flank downdraft momentum surges in the 18 May 2010 Dumas, Texas, supercell. *Mon. Wea. Rev.*, **142**, 2935–2960, doi:10.1175/MWR-D-13-00240.1.

Straka, J. M., E. N. Rasmussen, R. P. Davies-Jones, and P. M. Markowski, 2007: An observational and idealized numerical examination of low-level counter-rotating vortices in the rear flank of supercells. *Electron. J. Severe Storms Meteor.*, **2** (8), http://www.ejssm.org/ojs/index.php/ejssm/article/viewArticle/32.

Thompson, R. L., C. M. Mead, and R. Edwards, 2007: Effective storm-relative helicity and bulk shear in supercell thunderstorm environments. *Wea. Forecasting*, **22**, 102–115, doi:10.1175/WAF969.1.

——, B. T. Smith, J. S. Grams, A. R. Dean, and C. Broyles, 2012: Convective modes for significant severe thunderstorms in the contiguous United States. Part II: Supercell and QLCS tornado environments. *Wea. Forecasting*, **27**, 1136–1154, doi:10.1175/WAF-D-11-00116.1.

Wicker, L. J., and R. B. Wilhelmson, 1995: Simulation and analysis of tornado development and decay within a three-dimensional supercell thunderstorm. *J. Atmos. Sci.*, **52**, 2675–2703, doi:10.1175/1520-0469(1995)052<2675:SAAOTD>2.0.CO;2.

——, and W. C. Skamarock, 2002: Time-splitting methods for elastic models using forward time schemes. *Mon. Wea. Rev.*, **130**, 2088–2097, doi:10.1175/1520-0493(2002)130<2088:TSMFEM>2.0.CO;2.

Wilhelmson, R. B., and C.-S. Chen, 1982: A simulation of the development of successive cells along a cold outflow boundary. *J. Atmos. Sci.*, **39**, 1466–1483, doi:10.1175/1520-0469(1982)039<1466:ASOTDO>2.0.CO;2.

Wurman, J., D. Dowell, Y. Richardson, P. Markowski, E. Rasmussen, D. Burgess, L. Wicker, and H. B. Bluestein, 2012: The second Verification of the Origins of Rotation in Tornadoes Experiment: VORTEX2. *Bull. Amer. Meteor. Soc.*, **93**, 1147–1170, doi:10.1175/BAMS-D-11-00010.1.

Ziegler, C. L., 1985: Retrieval of thermal and microphysical variables in observed convective storms. Part I: Model development and preliminary testing. *J. Atmos. Sci.*, **42**, 1487–1509, doi:10.1175/1520-0469(1985)042<1487:ROTAMV>2.0.CO;2.